ISSN 1562 - 2703

INTERNATIONAL JOURNAL AUTOMATION AUSTRIA

Heft 2 im Jahrgang 22 (2014)

Inhalt *Seite*

SCOPE

"International Journal Automation Austria" (IJAA) publishes top quality, peer reviewed papers in all areas of automatic control concerning continuous and discrete processes and production systems.

Only original papers will be considered. No paper published previously in another journal, transaction or book will be accepted. Material published in workshops or symposia proceedings will be considered. In such a case the author is responsible for obtaining the necessary copyright releases. In all cases, the author must obtain the necessary copyright releases before preparing a submission. Papers are solicited in both theory and applications

Before preparing submissions, please visit our instructions to authors (see back cover) or web page.

International Journal Automation Austria also is the official executive authority for publications of IFAC-Beirat Österreich.

Imprint: Propagation of Automatic Control in Theory and Practice.

Frequency: Aperiodically, usually twice a year.

Publisher: IFAC-Beirat Österreich, Peter Kopacek, Alexander Weinmann

Editors in Chief: Alexander Weinmann, Peter Kopacek

Address: 1) Institut für Automatisierungs- und Regelungstechnik (E376), TU Wien, A-1040 Wien, Gußhausstrasse 27-29, Austria
Phone: +43 1 58801 37677, FAX: +43 1 58801 37699
email: danzinger@acin.tuwien.ac.at
Homepage: http://www.acin.tuwien.ac.at/publikationen/ijaa/

2) Intelligente Handhabungs- und Robotertechnik (E325/A6), TU Wien, A-1040 Wien, Favoritenstrasse 9-11, Austria
email: e318@ihrt.tuwien.ac.at

Layout: Rainer Danzinger
Printing: Grafisches Zentrum an der TU Wien

Design and Optimisation of the Joint Controllers of a Humanoid Robot.

M. Schörghuber, F.d'Apolito and P.Kopacek
Vienna University of Technology, Austria
Institute for Mechanics and Mechatronics, IHRT
Favoritenstrasse 9-11/E325 A6, A – 1040 Wien
markus.schoerghuber@gmx.net; francesco.dapolito08@gmail.com;
kopacek@ihrt.tuwien.ac.at

Abstract: Humanoid robots are on the way to be used more and more in industry especially in the intelligent production e.g "Production 4.0". Currently there are nearly no humanoid robots available for such applications. One of the main barriers is the price and the availability of such robots. Therefore "Cost Oriented Humanoid Robots – COHR" are necessary in the nearest future.

Therefore in this paper, as one step towards COHR, the control of the joints of a humanoid robot by means of currently commercially available microcontrollers is described. Starting with an experimental identification on an existing robot with joints consisting of brushless or brushed DC motors and harmonic drives the optimal controller parameters for simple, time discrete, digital P- and PI- controllers are derived for a three - cascaded (current, velocity, position) control architecture. Because of nonlinearities the velocity controller have to be "adaptive" – the gain depends from the velocity – called piece-wise linear controller first introduced in 1978.

Tests on an existing humanoid robot show very good results. Finally an outlook of further improvements concerning the control of this robot and similar COHR robots is given.

Keywords: *Humanoid robots, control, system identification.*

1. Introduction

There are a lot of publications dealing with the control of humanoid robots available in the literature mostly from authors with an IT background. Only few of them describe this problem from the viewpoint of control engineering and present only simulation results. Therefore the main goal of this contribution is to get a model of a robot joint by means of an experimental identification. Based on this model industrial controllers will be optimized with "classical" methods of control engineering.

One of the differences to other publications is the availability of a real cost oriented humanoid robot (COHR) named Archie, developed at IHRT in the last years for testing the results on a real system. According to the philosophy "cost oriented" most of the parts are available on the market for reasonable costs (Kopacek, 2011). Details of this robot are available e. g. (Schörghuber and Kopacek, 2014). The results can be easy transferred to other humanoid robots.

The control system design of this humanoid robot is implemented following the idea of a hierarchically control architecture consisting of a high- and a low-level control structure. The high-level control structure is responsible for the overall motion planning and sends the calculated position and velocity commands to each of the robot's joints. These joints, the low level control, consist of a DC-motor, a gear and a micro-controller. The overall stability of the robot during walking depends mainly on the precise execution of the position and velocity commands sent to each of the robot's joints.

In order to analyze and optimize the overall stability of the robot the dynamic behavior of the joints will be investigated by means of an experimental system identification. All joints, except for the right and left transversal hip joints, are actuated by a brushless DC-motor. Since the construction of these joints, namely the right frontal and sagittal hip joints, the right sagittal knee joint and the right sagittal and frontal ankle joints, is identical, the results of the system identification are valid for all of these joints. Based on the results of the system identification the low-level controllers will be designed in order to ensure a precise execution of the position and velocity commands. Due to the symmetric structure of the robot, the controller design for the joints in the right part of the robot can be applied for the left part as well. Therefore, only the controllers for the joints shown in Figure 1 will be taken into account.

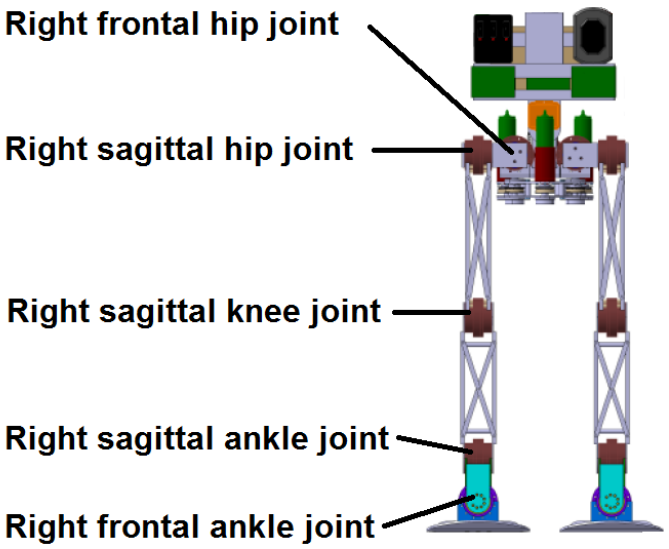

Figure 1: The included robot's joints

2. The robot Joints

Humans have muscles to actuate one to three joints degrees of freedom – DOF`s of one joint . Trying to copy a human muscle, the robot's joints need to fulfill the following requirements:

- High torque

- Ability to operate in a wide velocity range
- Small size
- Light weight

Currently there are no appropriate artificial muscles available. Probably by means of Nano- and Femtotechnology such drives will be available in the nearest future. But now every DOF in the robot's mechanical structure is actuated either by a brushed or a brushless DC-motor combined with a gear and a controller. In our case most of the joints are actuated by a brushless DC-motor with a "Harmonic Drive" gear, the remaining are actuated by a brushed DC-motor using a belt drive.

A brushless DC-motor offers various advantages compared to a brushed DC-motor, such as a smaller motor size, higher efficiency, less weight, less maintenance, longer life time and a good torque-to-rotational-speed characteristic.

The used brushless industrial DC-motor has the specifications listed in Table 1.

Power	50 [W]
Nominal voltage	24 [V]
Max. continuous torque	82.7 [mNm]
Max. peak torque	822 [mNm]
Max. continuous current	2.32 [A]
Max. peak current	23.3 [A]
Max. rotational speed	10000 [min^{-1}]
Number of pole pairs	8
Number of phases	3
Weight	110 [g]

Table 1. Datasheet Maxon E 45 flat (Maxon, 2014)

For the exact determination of the actual position of the rotor, the brushless DC-motor is equipped with three Hall sensors.

To operate the brushless DC-motor in the robot joints an industrial digital micro-controller (Elmo, 2013) was chosen. This micro-controller reflects a standardized commercial device that can be applied in various industrial applications, such as robots or other complex machines with a three-cascaded digital control architecture to control the current, velocity and position of the brushless DC-motor.

Fig.2 shows the system architecture of the micro-controller including the communication possibilities via a CAN-network or via the RS-232 communication protocol (Elmo 2013).

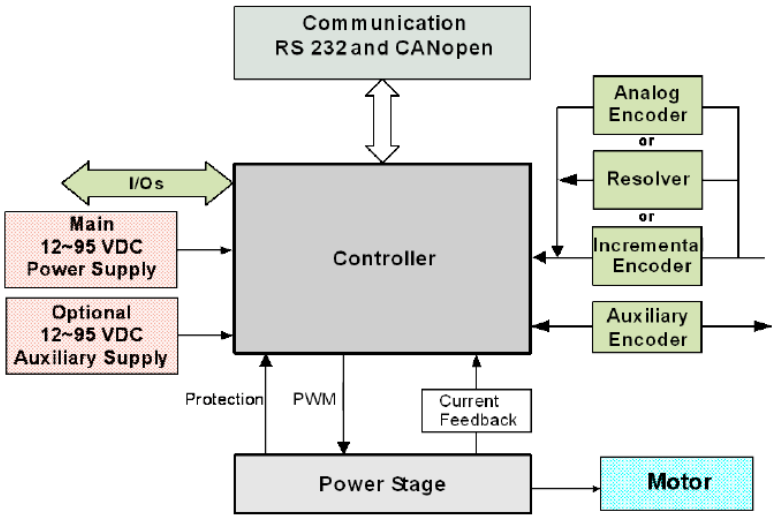

Figure 2. Micro-controller system architecture (Elmo, 2013)

The control of the whole robot is realized as decentralized control system as shown in Fig. 3. The walking pattern planner calculates the food placements and trajectories based on position and velocity feedback of the torso. Then the joints angle trajectories are calculated by inverse kinematics transforming the walking trajectories from cartesian to joint space (Bajrami, 2013).

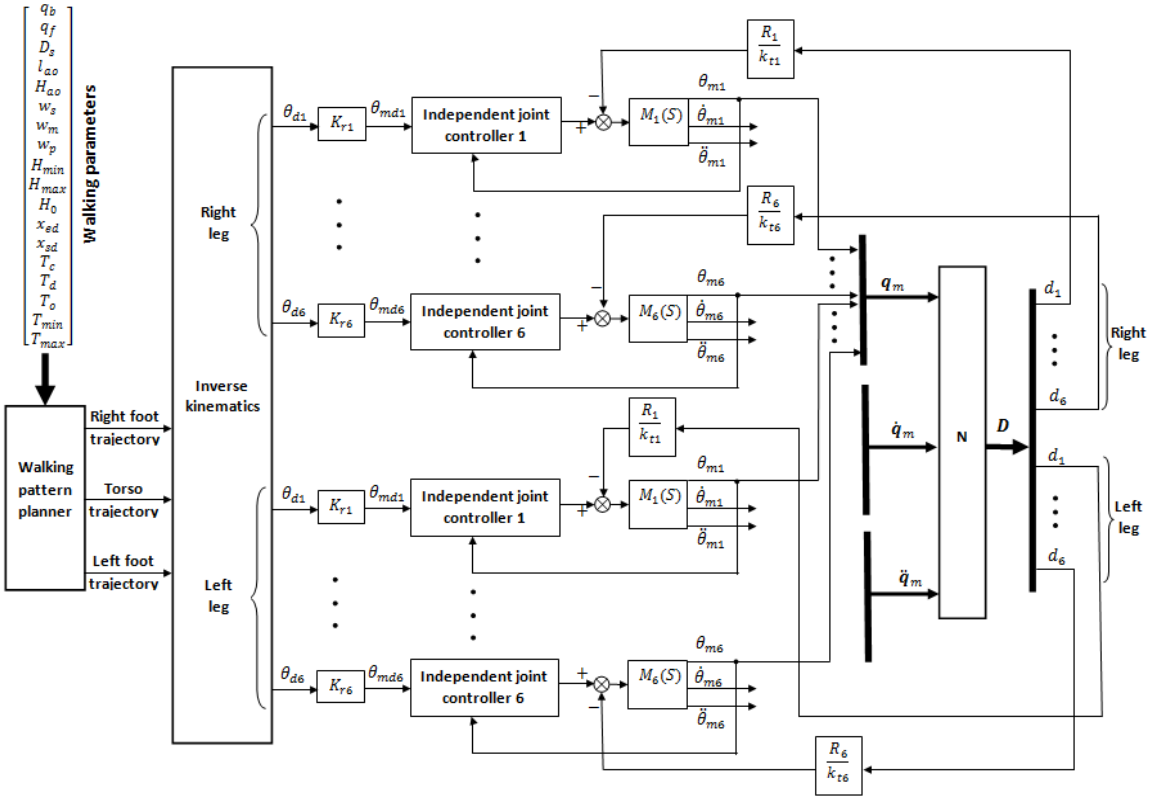

Fig. 3 Overall Control System (Daniali, 2013)

3. System Identification

The system identification will be performed by analyzing the dynamic response of the robot's right knee joint according to specific test signals. Since all of the robot's joints actuated by brushless DC-motors have an identical structure and therefore a similar dynamic behavior, the results of the system identification can be easily transformed of the other joints.

As a first step of modeling the system brushless DC-motor, harmonic drive gear and the adjacent mechanical structure, the basic model structure, the individual parts and the connections between them will be investigated. The system input variable is represented by the active current delivered by the micro-controller which is then transformed by the DC-motor into a mechanical rotation of the DC-motor's rotor with a certain torque. These mechanical parameters, the angular velocity and the torque are then transformed further by the harmonic drive, decreasing the velocity and increasing the torque.

Because a linear system identification yields to insufficient results a nonlinear system identification using a Hammerstein model was used.

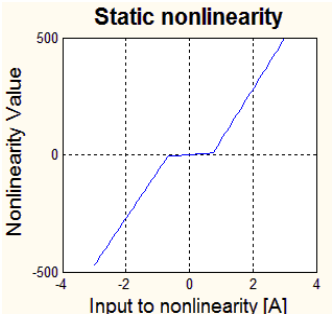

Fig.4 Static Nonlinearity (Schörghuber, 2014)

The result of the system identification shows that the dynamic behavior of the joints is a first order lag element with a dead zone and a nonlinear gain (Fig.4). In order to deal with the nonlinear gain the gain scheduling function implemented in the micro-controller is used and the joint controllers are tuned in 64 working points. Summarizing the results of the system identification:

- The robot's joints are nonlinear.
- The nonlinearity is static and consists of a dead zone from the friction, a velocity dependent gain.

4. Design of the Joint Controllers

The goal of this chapter is to design optimal controllers for all of the robot joints actuated by brushless DC-motors. All of the robot joints are controlled using the same micro-controller, as described before. For these digital controllers optimal parameters for the three-cascaded control loops must be determined ensuring a accurate, stable control with no overshooting.

Figure 5 shows a block diagram of the used three-cascaded control architecture although the Figure does not explicitly show the current controller feedback from the connected DC-motor. In addition, the Fig. shows the functional principle of the gain scheduling algorithm and of the position command feed forward bloc.

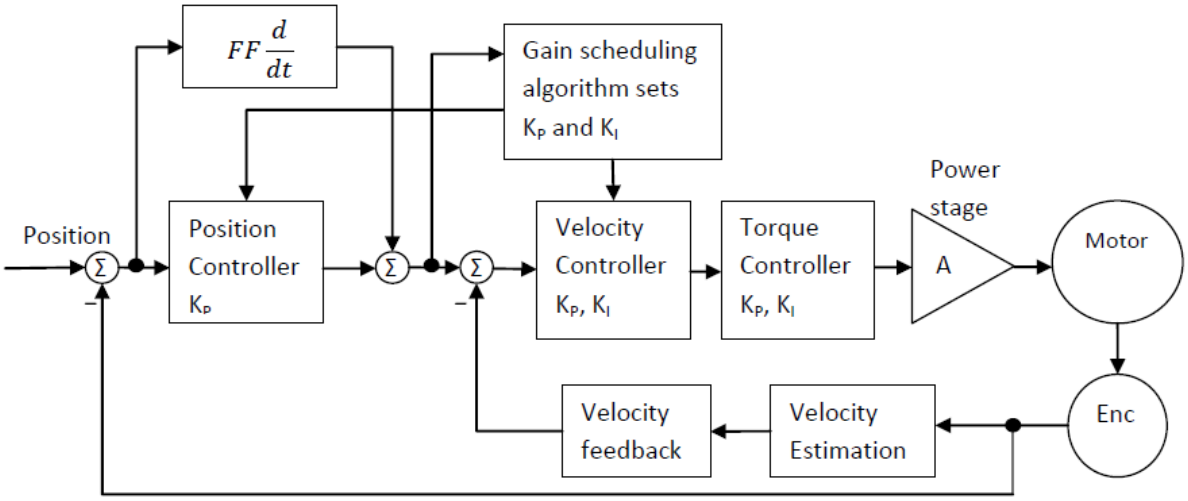

Fig. 5 Three cascaded control architecture (Schörghuber, 2014)

In Fig.5 the inner loop is the current control loop realized by a standard PI-Controller. The middle control loop - the velocity control loop is realized by a PI-controller with an adaptive gain – piecewise linear controller - according to the nonlinearity. For the outer control loop, the position control loop, only a simple P-Controller (Elmo, 2011) is necessary.

According to the identification the sampling time of the current control loop is chosen with 90msec which is sufficient to cover the whole bandwidth of the dynamic behavior of the robot joints and still leaves enough CPU power to guarantee a stable control behavior. For the velocity loop 180msec and for the position loop 360msec were chosen.

For the tuning of the current control loop the micro-controller offers an auto tuning function implemented in the software. After providing the basic motor parameters the auto tuning function energizes the motor winding with a high frequency current in order to identify the dynamic response of the DC-motor. The motor parameters, specifically resistance and inductance of the motor windings, are estimated and the PI-controller is tuned accordingly.

The controller parameters resulting from the auto tuning function yield to a stable control. After some manual adjustments the optimal controller parameters for a sufficiently fast control with no overshooting are listed in Tabs. 2a - c.

Current Controller					
Joint	**Hip Frontal**	**Hip sagittal**	**Knee sagittal**	**Ankle frontal**	**Ankle sagittal**
Controller type	PI-controller				
Sampling time [msec]	TS = 90				
Gain Kp	1.386	1.316	1.352	0.316	1.358
Integral gain KI [s^{-1}]	2250	2332	2312	1243	2578
Rise time	Faster than measureable				
Overshoot	none				
Settling time	Faster than measureable				

Table 2a: Optimal parameters for the current controller

In this table the optimal controller parameters for hip, knee and ankle for the optimized linear PI controllers are listed. All of them are similar except for the ankle frontal. The reason is the small movements of the ankle in this direction.

The velocity controller is realized also by a digital proportional integral controller (PI-controller). According to Fig. 4 different linear controllers for various working points can be used in the working range of interest. In practice, this means that the control gains of the velocity controller need to be adjusted depending on the desired velocity of the joints. Such, so called “Piece-wise” linear PI controllers, with an “adaptive” gain, were used very early for industrial applications e.g. for air conditioning control in glass houses (Kopacek and Pillmann, 1978).

Velocity Controller	
Controller type	Piece-wise linear PI-controller
Sampling time [msec]	TS = 180
Gain	Dependent on the velocity
Integral gain	Dependent on the velocity
Rise time	Dependent on the velocity
Overshoot	none
Settling time	Dependent on the velocity

Table 2b: Optimal parameters for the velocity controller

For velocities 0,94 deg/sec to 63 deg/sec the maximum and minimum values of the gain and the integral gain are listed in Tab. 3

	Hip front	Hip sag	Knee sag	Ankle front	Ankle sag
Kp	900-400	900-400	1000-150	1200-600	800-400
KI	70000-10000	70000-10000	450000-5000	140000-50000	52000-15000

Tab.3 Gain and integral gain for the velocity controller

The position controller is piece-wise linear P-Controller and optimized for a small overshooting and a minimum of the position error. For this purpose, it is accurate enough to split the velocity range into two parts, choosing only two different controller gains.

Position Controller	
Controller type	Piece-wise linear P-Controller
Sampling time [msec]	360
Proportional Gain	For velocities > 200 [counts/sec] KP = 5 For velocities < 200 [counts/sec] KP = 3
Rise time	Depending on the position command
Overshoot	none
Settling time	Depending on the position command

Table 2c: Optimal parameters for the position controller

According to the headline “Cost Oriented Humanoid Robots – COHR” simple industrial controllers can be used for the control of the nonlinear robot joints. The main disadvantage of those controllers is the volume and the weight of currently available hardware.

5. Validation & Conclusion

The validation is performed using the trajectories for the actual walking pattern. As an example the results for the knee are shown in Figs.6a-c. Fig.6a show the actual position vs. the position command , Fig.6b the position error and Fig 6c the actual velocity vs. the velocity command .

The control deviation for the position is minimised – no differences in Figs. 6a,b. For the velocity a small control deviation occurs (Fig.6c).

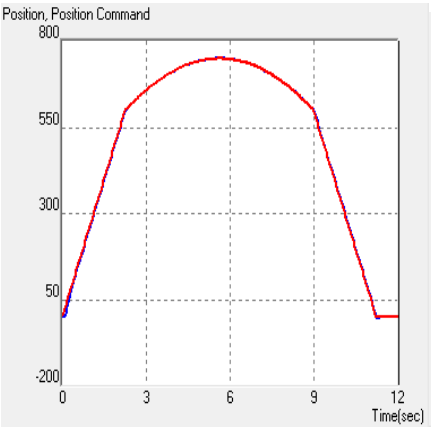

Fig. 6a

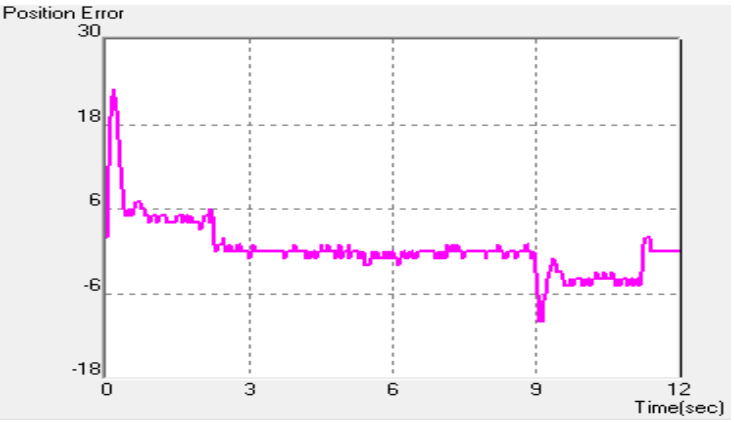

Fig. 6b

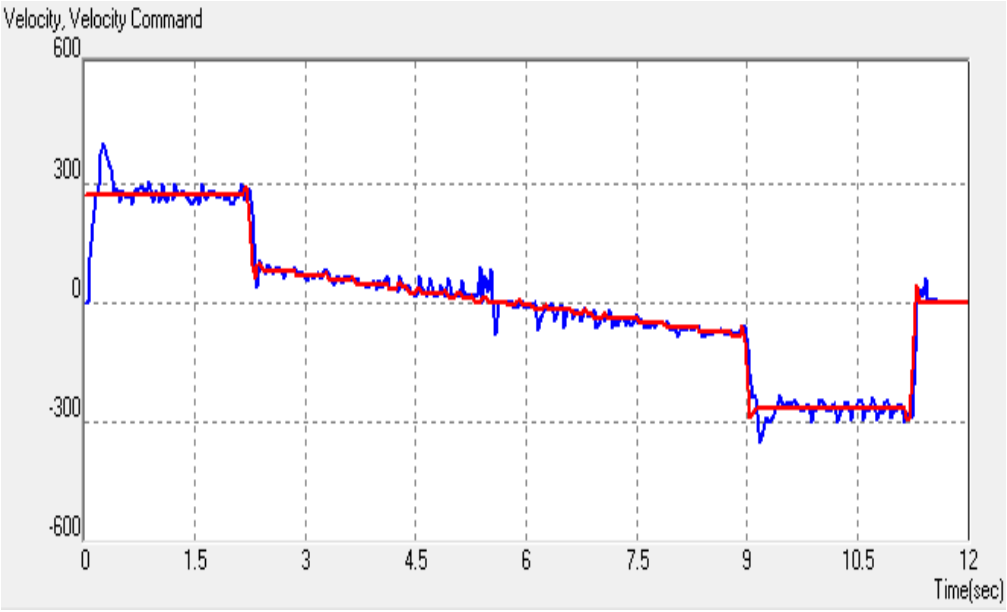

Fig. 6c

Fig. 6a – c: Trajectories commands vs. actual trajectories for the knee joint (Schörghuber, 2014)

The gain scheduling function enables a very accurate performance of the position and velocity commands despite the nonlinear gain of the robot joints. Due to the dead zone nonlinearity the joint has difficulties to operate at very low velocities and therefore the trajectories for the robot should be designed accordingly.

6. Summary

The robot's joints are composed of a DC-motor and a gear set and are controlled by a standardized commercial micro-controller. The micro-controller uses certain position reference modes, namely the Position Time (PT) and the Position Velocity Time (PVT) mode, that can be programmed by the user. A mathematical model of the underlying physical system is derived by means of system identification.

- The robot's joints are nonlinear.

- The nonlinearities are static and consist mainly of a dead zone and a nonlinear gain as a function the velocity.

- The nonlinearities came from the friction in the gear as a function of the velocity and by the nonlinear dynamics of the DC-motor.

The micro-controller uses for the joints a three-cascaded control with loops for the current, the velocity and the position. The position feedback signal is measured by digital Hall sensors added on the DC-motor and the velocity feedback signal is calculated based on this position signal.

- The validation of the tuned controllers for the robot's joints is performed using the actual trajectories for the walking patterns of the robot and shows the following results:

- The gain scheduling function of the industrial controller yields to a basic parameter set. Manual adoptions are necessary to reach an optimum for the position and velocity control.

- The dead zone nonlinearity makes it difficult for the DC-motor to operate at very low velocities. This problem is most likely caused by the friction of the gear and cannot be resolved by the controller. The sole way to cope with the dead zone nonlinearity is to design the trajectories for the various joints in such a way that very low velocities are avoided wherever possible.

- A rapid change of the position commands leads to a significant velocity overshoot. This effect has to be accepted to achieve a high position accuracy but can be circumvented by avoiding rapid velocity changes when designing the trajectories for the various joints.

- The frontal ankle joint is rarely moved but has to be kept in the same position most of the time during a movement of the robot. Since this joint is the lowest joint of the robot a high torque needs to be produced to keep all of the above mechanical structure in the same position, preventing the DC-motor from rotating. This causes the DC-motor to overheat and damages the electrical components significantly, resulting in an altered and poor dynamic behaviour of this joint.

7. Outlook

As a matter of facts, a new high level control structure for the humanoid robot Archie is currently under development. It is basically an upgrade of the existing software. The need for a new software came from the next steps in the development of Archie such as the possibility to add a vision system or other sensors in order to improve Archie's walking capabilities and the result of the research described in this paper.
Since Archie is still not equipped with cameras, the new software will check the presence of cameras by use of the CAN bus connection with the robot. In case there are cameras, the software will wait for the pictures sampled by the cameras sent by Archie via the CAN bus driver and after it receives them, the software will distinguish between area with no obstacles, areas where Archie can step over an obstacle and areas that Archie has to avoid. Afterwards the software will perform two kinds of planning:

- a gait planning that will be used to plan the optimal path and
- a step planning performed afterwards that will be used to perform the planning of the positions and the velocities of the joints.

The software, with the images coming from the cameras, will create a map with different colors: green for an obstacles free area, orange for the areas where Archie can step over the obstacles and red for the areas that Archie has to avoid. This colored map will be created studying adjacent points and computing the slope between these two adjacent points.

The general planning consists basically on the planning of the center of gravity and of the ZMP of the robot. Every ZMP computed in this way will be considered by the software as the new goal, considering as start position the previous ZMP in the path.

When Archie is in a green area, the step planning method will be called. The algorithm will compute the positions and the velocities of the joints and will send them to Archie via the CAN bus driver in the form of a PVT table together with the relative velocity gains mentioned above. When Archie is in an orange area, the step planning will be called , adding the position of the obstacle it has to step over, and then, the computed positions and velocities will be sent to Archie via the CAN bus driver in the form of a PT table together with the velocity gains.

If there are not cameras then the user will have to choose the direction Archie has to move, how many steps it will have to do and if there is an obstacle in front of it. After this choices are done the software will compute the ZMP points depending on the input variables and then, for every step, the step planning function will be called.

References

Bajrami, Xh., (2013).Dynamic Modelling and Simulation of a Biped Robot, *PhD Thesis, Vienna University of Technology,* 2013.

Byagowi, A., (2010). Control System for a Humanoid Robot, *PhD Thesis, Vienna University of Technology*, 2010.

Daniali, M., (2013). Walking Control of a Humanoid Robot, *PhD Thesis, Vienna University of Technology,* 2013.

Elmo, Motion Control (2011), *SimplIQ Software Manual*, Ver. 1.4.

Elmo, Motion Control (2013), *SimplIQ Line - Whistle and Tweeter Digital Servo Drives Installation Guide*, Ver. 1.603.

Kopacek,P.; W.Pillmann (1978): A Nonlinear Cascade Controller for Air Conditioning Plants. *In: Preprints of the 7th IFAC World Congress, Helsinki, 1978*, Vol. I, p.335-342.

P.Kopacek (2011): Cost Oriented Humanoid Robots; *Proceedings of the 18th IFAC World Congress Milano (Italy) August 28 - September 2, 2011*, p. 12680- 12685; DOI 10.3182/20110828-IT1002.0156.

Kopacek,P.; M.Schörghuber and J. Baltes (2014): A Cost Oriented Humanoid Robot Motion Control System. *Preprints of the 19th World Congress. The International Federation of Automatic Control Cape Town, South Africa. August 24-29, 2014*, p.4529 – 4534.

Maxon (2014), *Product catalogue*,http://www.maxonmotor.com/medias/sys_master/8807046709278/13-221-EN.pdf. Last viewed 12 April 2014.

Schörghuber, M., (2014). Controller Design of a humanoid robot, *Master Thesis, Vienna University of Technology*, 2014.

Horizon-Respective Robustness of Model Predictive Control

Alexander Weinmann, OVE, Life Senior Member IEEE
Vienna University of Technology, Institute of Automation and Control
Gusshausstrasse 27-29/376, A-1040 Vienna / Austria
Phone: +43 1 58801 37611, Fax: +43 1 58801 37699
email: weinmann@acin.tuwien.ac.at

Manuscript received October 11, 2014

Abstract

The prediction horizon does not only influence the traditional performance of the Model Predictive Control but also robustness and sensitivity parameters. Some correspondences yield an additional design option for an over-all operation quality in the field of industrial applications.

Keywords: Sensitivity and robustness features, prediction horizon, maximum deviation modulus for high matrix power

1 Introduction

Model predictive control aims at including future control signals into the control activities in order to minimize a square index of performance on the control deviation and actuating variable. Including fewer inputs always reduces the overall quality of the control system, and vice versa.

However, model uncertainties cause deviations in the predicted operations; due to higher powers of the system coefficient matrix, less quality is to be expected when looking farther into the fucture of the system behavior. When increasing the horizon, disadantageously the sensitivity is increased although the future prediction is improved. Thus, these facts have to be balanced versus each other.

The goal of this paper is to put emphasis on the uncertainty-driven defects on prediction quality. There are a lot of irregular properties when studying the results of the Model Predictive Control referring to the prediction horizon. However, there are some properties to be detected which are worth while to be utilized to obtain robust behavior.

2 Basic Observations

2.1 Influence of the Prediction Horizon

A typical result of the influence of the horizon paramter $n_y,\ n_u$, see Appendix B, and of the uncertainty of $\mathbf{\Phi},\ \mathbf{\Psi},\ \mathbf{C}$ on the maximum absolute value of Model Predictive Control gain is given in Fig. 1. Three different uncertainties have been chosen with different influence magnitude. Distinct jumps are possible when studying the dependence on n_y.

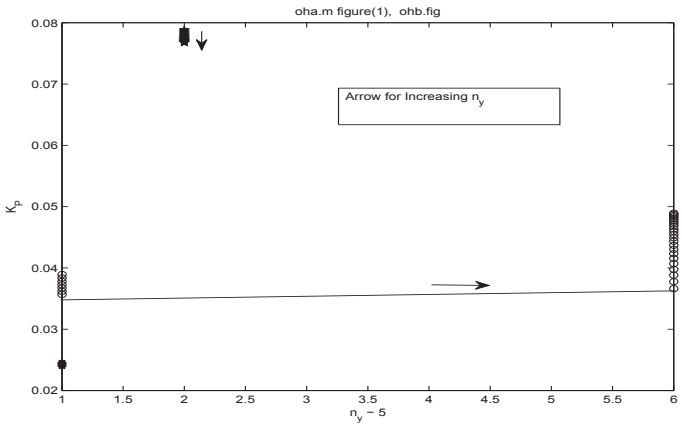

Figure 1: Prediction horizon n_y and uncertainty influence on the gain $\mathbf{K}_P$

The influence of n_y on the maximum absolute value of the elements of the deviation of $\Delta\mathbf{K}_P$ is rendered in Fig. 2. Three uncertainties are established in the plant. In Fig. 2, the horizon is varied up to some n_y. Then, that $n_y \stackrel{\triangle}{=} n_y|_{max}$ is detected where $|\Delta\mathbf{K}_P|$ is maximum. This result is depicted in Fig. 2 with twelve subfigures for increasing amount of uncertainty.

In this example, labelled with a dot, the first uncertainty is introduced in the sixth element of the diagonally implemented $\mathbf{\Phi}$. The second uncertainty, labelled with a star, is introduced in the fifth element of the vector-valued $\mathbf{\Psi}$. The third uncertainty, labelled with a pentagram, is the fourth element of the vector-valued $\mathbf{C}$. For the first uncertainty, the maximum absolute value of the elements of the deviation of $\mathbf{K}_P$ varies with n_y in Fig. 2, the other uncertainties have only low influence. for the other uncertainties the maximum is always arrived at $n_y = 6$. For larger uncertainties, the maximum deviation

in $\mathbf{K}_P$ is arrived at smaller n_y, yet. Hence, it is not worth while to select a bigger horizon in the case of larger uncertainties.

Keep an eye on the arrows in Fig. 2, plotted, e.g., in the last subfigure. The twelve subfigures are plotted for increasing size of the uncertainty. However, the plotted dots indicate the maximum deviation at the appropriate n_y. The motion is characterized by distinct jumps. For small uncertainties, subfigure 1 to 6, $\max|\Delta K_{Pi}|$ increases with n_y; for higher and increasing uncertainties, subfigure 7 to 12, n_y decreases with the location of $\max|\Delta \mathbf{K}_{Pi}|$.

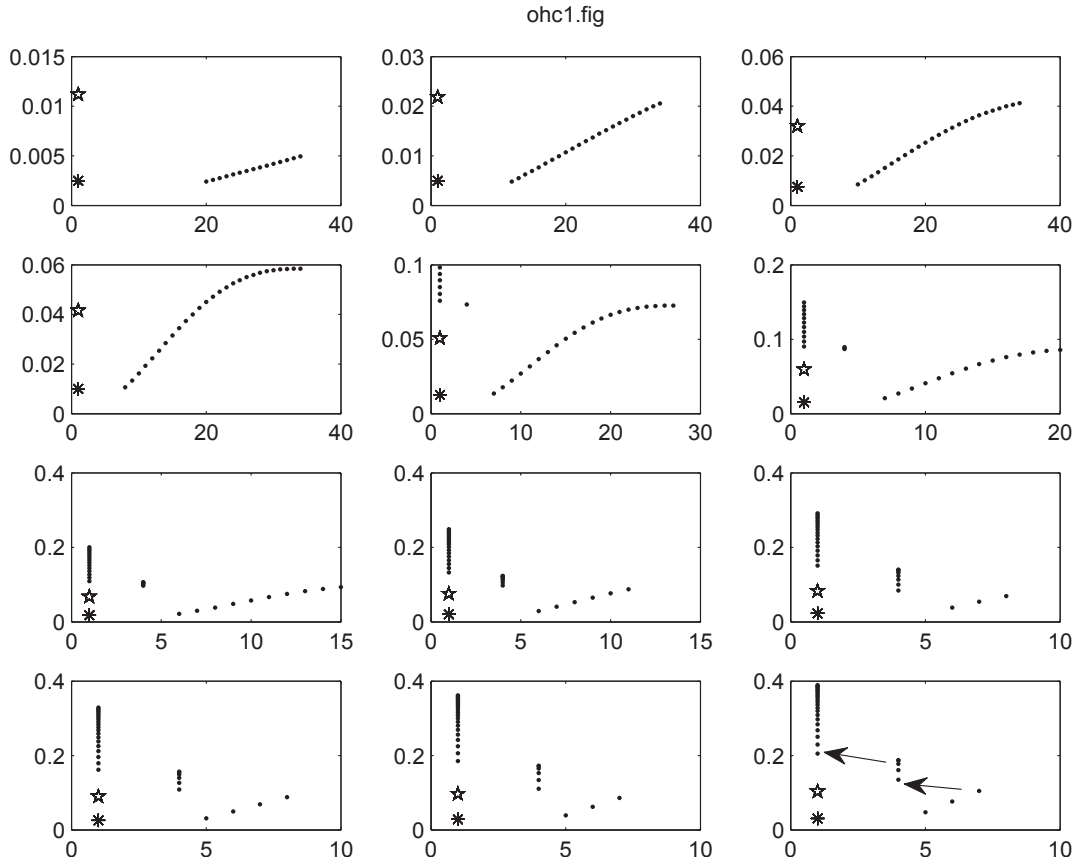

Figure 2: Distribution of the maximum deviation modulus of $\Delta\mathbf{K}_P$ versus appropriate $(n_y - 5)_{max}$ for three uncertainties $\cdot, *$, pentagraph; Abscissa $(n_y - 5)|_{max}$

For some different setup, the other uncertainties also cause a remarkable influence on $\Delta\mathbf{K}_P$, see Fig. 3.

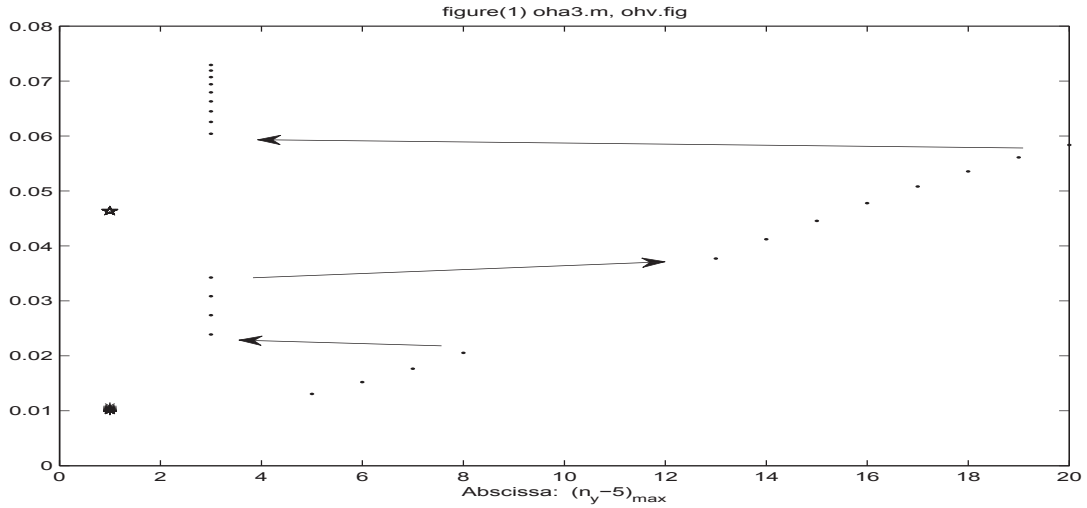

Figure 3: Distribution of the maximum absolute value of the elements of the deviation $\Delta\mathbf{K}_P$ versus appropriate $(n_y - 5)_{max}$ for three uncertainties

2.2 Dependences on the Prediction Horizon

Consider a typical example

$$\mathbf{\Phi} = \begin{pmatrix} 1 & 0 & 0 & 0.01 & 0 & -0.2 \\ 0.4 & 0 & 0 & 0 & 0 & 0 \\ 0.4 & 1 & 0 & 0 & 0 & 0 \\ 0.4 & 0 & 1 & 0 & 0 & 0 \\ 0.4 & 0 & 0 & 1 & 0 & 0 \\ 0.4 & 0 & 0 & 0 & 1 & 0 \end{pmatrix}, \quad \mathbf{\Psi} = \begin{pmatrix} 7.3 & 1 \\ 2.9 & 2 \\ 5.1 & 3 \\ 6.2 & 1 \\ 6.7 & 4 \\ 6.9 & 0 \end{pmatrix}, \quad \begin{array}{l} \mathbf{C} = \begin{pmatrix} 0 & 0 & 0 & 0 & 0 & 1 \end{pmatrix}, \\ \mathbf{Q} = 9\mathbf{I}_{r\,n_y}\ , \\ \mathbf{R} = \mathbf{I}_{m\,n_u}\ , \\ m = 2 \end{array} . \tag{1}$$

A graph is plotted for some low n_y. Afterwards a next graph is plotted for $n_y + 1$ etc. while the former one is hold on. Finally, a superposition $\forall n_y$ is produced in Fig. 4, lower part. A zoomed selection for $n_y = \{1, \ldots 11\}$ is given in the upper part.

Several further results, e.g., the transients of $\mathbf{H}_P$ and $\mathbf{F}_P$ are given in Fig. 5. Note the different slow-down envelopes in Figs. 6 and 7. What you find confirmed and what is also to be expected is that the results are very sensitive in a medium scale region.

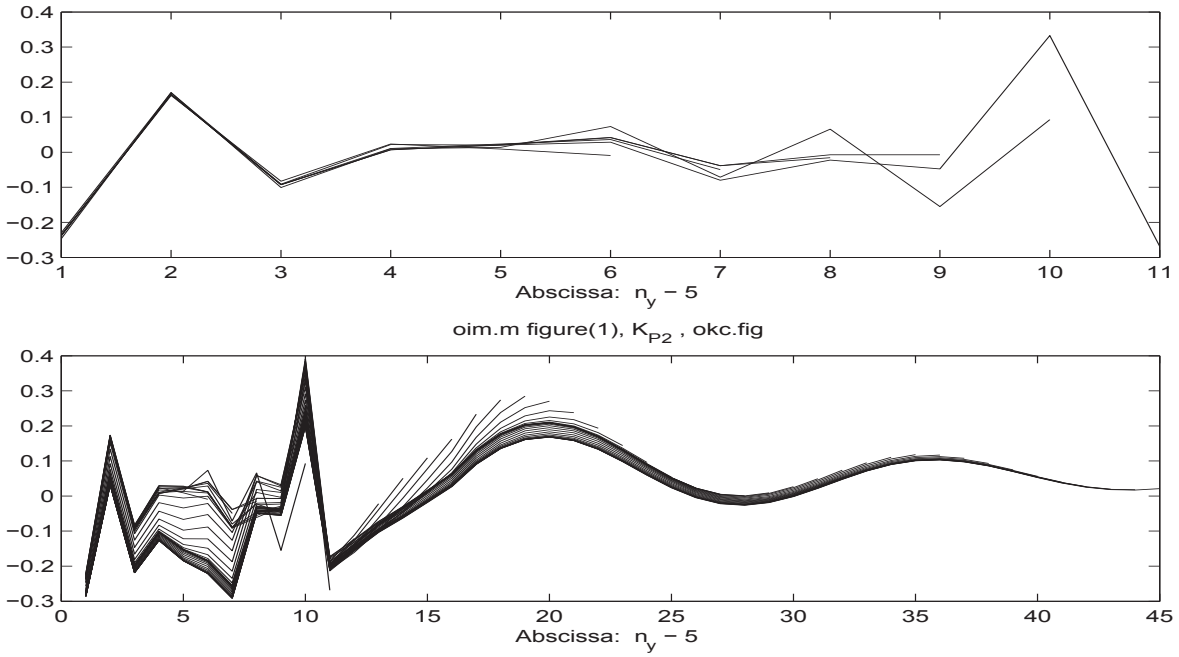

Figure 4: Second component of $\mathbf{K}_P$ versus $n_y = \{1, \ldots n_y - 5 = 45\}$.

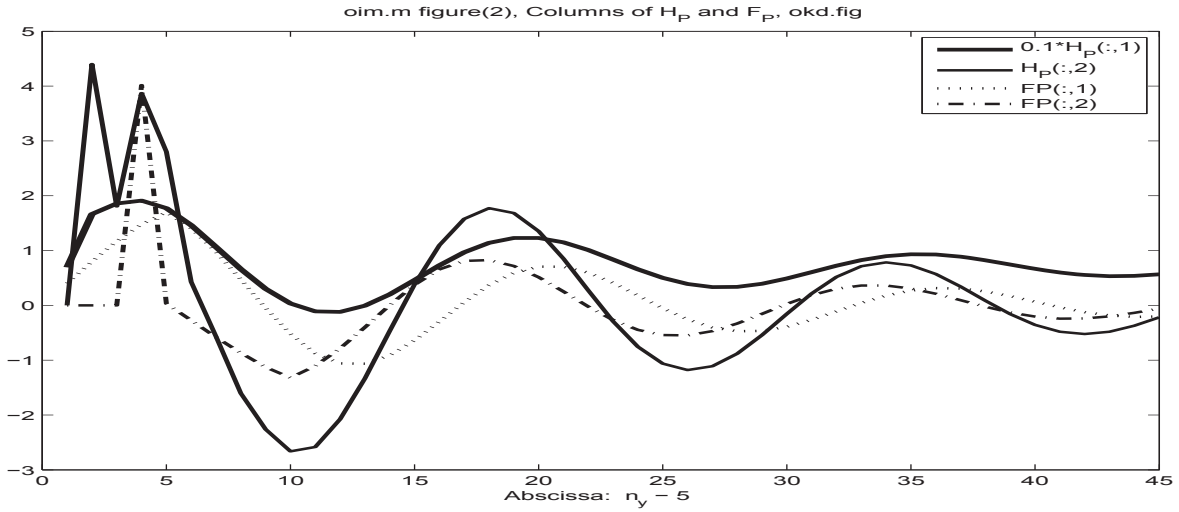

Figure 5: Both components of $\mathbf{H}_P$ and $\mathbf{F}_P$

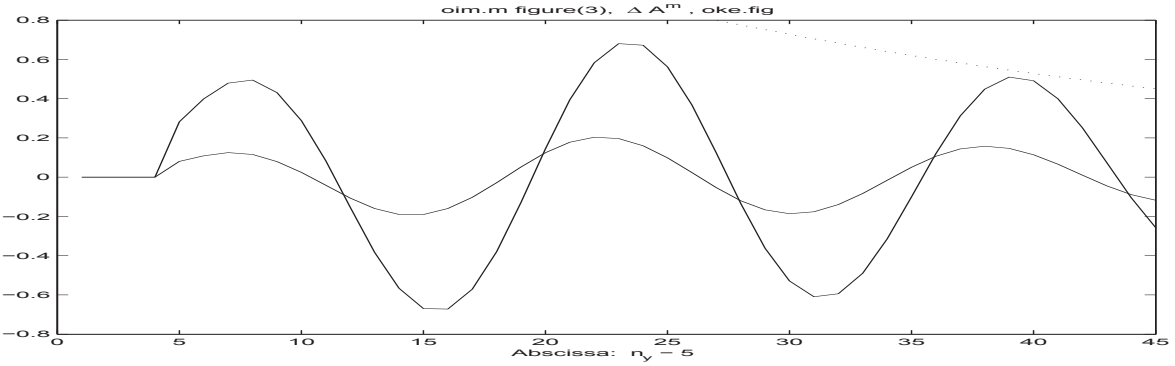

Figure 6: Both components of the sensitivity [Eq.(17)] $\mathbf{C} \cdot \ (\sum_i \mathbf{\Phi^i} \cdot \Delta\mathbf{\Phi^i} \cdot \cdot \mathbf{\Phi}^{n_y - i})\ \mathbf{\Psi}$ for $\Delta\mathbf{\Phi} = \mathbf{0}_6$ except $\Delta\Phi(1,4) = 0.1$ versus the prediction horizon

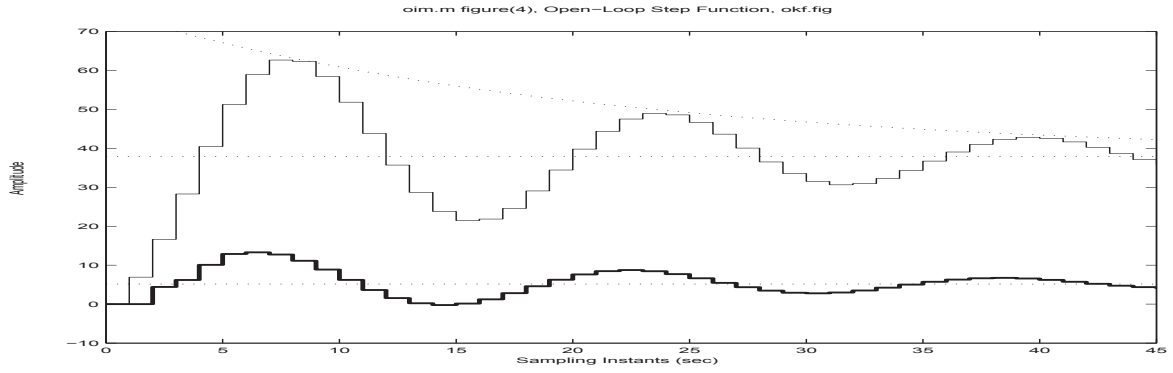

Figure 7: Both outputs of the open-loop `dstep`, for illustration

3 Model Predictive Control Eigenvalues and Prediction Horizon

3.1 Characteristic Equation, z-Domain

Based on $\mathbf{x} \in \mathcal{R}^n$; $\mathbf{y} \in \mathcal{R}^r$; $\mathbf{u} \in \mathcal{R}^m$; $\mathbf{A}, \mathbf{\Phi} \in \mathcal{R}^{n \times n}$; $\mathbf{B}$, $\mathbf{\Psi} \in \mathcal{R}^{n \times m}$; $\mathbf{C} \in \mathcal{R}^{r \times n}$; $\mathbf{K} \in \mathcal{R}^{m \times r}$; one finds for the linear discrete-time plant

$$\mathbf{x}(kT_s + T_s) = \mathbf{x}(k+1) = \mathbf{\Phi}(T_s)\mathbf{x}(k) + \mathbf{\Psi}(T_s)\mathbf{u}(k) \tag{2}$$

$$\mathbf{y}(kT_s) = \mathbf{y}(k) = \mathbf{C}\mathbf{x}(k) \tag{3}$$

$$\mathbf{\Phi}(T_s) = e^{\mathbf{A}T_s} \in \mathcal{R}^{n \times n} \quad \text{and} \quad \mathbf{\Psi}(T_s) = \mathbf{A}^{-1}[e^{\mathbf{A}T_s} - \mathbf{I}]\mathbf{B} \in \mathcal{R}^{n \times m}, \tag{4}$$

where $\mathbf{\Psi}$ results for a first-order hold and $\mathbf{A}$, $\mathbf{B}$ refer to the continuous-time basis.

Referring to the Appendix B, there are two resulting difference equations. We select $\mathbf{u}_{k,0} = \mathbf{u}_o$ and $\mathbf{x}_1$ as the initial condition. Then, for $k \geq 2$ one has

$$\mathbf{u}_k = (\mathbf{I}_m - \mathbf{K}_P\mathbf{G}_P)\mathbf{u}_{k-1} - \mathbf{K}_P\mathbf{F}_P\mathbf{x}_k - \mathbf{K}_P\mathbf{y}_{ref,k+1} \tag{5}$$

$$\mathbf{x}_{k+1} = \mathbf{\Phi}\mathbf{x}_k + \mathbf{\Psi}\mathbf{u}_k \ . \tag{6}$$

$$\text{In } z\text{-domain, } \mathbf{u}_k = z^{-1}\mathbf{u}_k - \mathbf{K}_P\mathbf{e}_k = z^{-1}\mathbf{u}_k - \mathbf{K}_P[\mathbf{F}_P\mathbf{x}_k + \mathbf{G}_P z^{-1}\mathbf{u}_k - \mathbf{y}_{ref,k+1}] \tag{7}$$

$$\mathbf{x}_k = bf\Phi z^{-1}\mathbf{x}_k + \mathbf{\Psi}z^{-1}\mathbf{u}_k \tag{8}$$

$$[\mathbf{I}_m(1 - z^{-1}) + \mathbf{K}_P\mathbf{F}_P(z\mathbf{I}_n - bf\Phi)^{-1}bf\Psi + \mathbf{K}_P\mathbf{G}_P z^{-1}]\mathbf{u}_k = \mathbf{K}_P\mathbf{y}_{ref,k+1}. \tag{9}$$

(For the single-input single-output and homogeneous case, we obtain an equivalent equation

$$[z\mathbf{I}_n - \mathbf{\Phi}z - \mathbf{\Psi}z(z - 1 + \mathbf{K}_P\mathbf{G}_P)^{-1}\mathbf{K}_P\mathbf{F}_P]\mathbf{x} = \mathbf{0}, \tag{10}$$

where $\mathbf{\Psi}$ and $\mathbf{K}_P^T$ are vectors, only.)

3.2 Sensitivity of MPC Eigenvalues

Consider the Eq.(9) for a two-valued input signal $\mathbf{u}_k$ in z-domain, where

$$\det[\mathbf{I}_m(1-z^{-1})+\mathbf{K}_P\mathbf{F}_P(z\mathbf{I}_n-\mathbf{\Phi})^{-1}\mathbf{\Psi}+\mathbf{K}_P\mathbf{G}_Pz^{-1}]=0 \tag{11}$$

provides the eigenvalues of the Model Predictive Control. The results are depicted in Fig. 8. There is a remarkable increase of the differential sensitivity versus the uncertainty for increasing n_y and a remarkable saturation, as well.

There is an explicit minimum at low $n_y = 9$. For increasing n_y the system approaches the stability boundary unit circle.

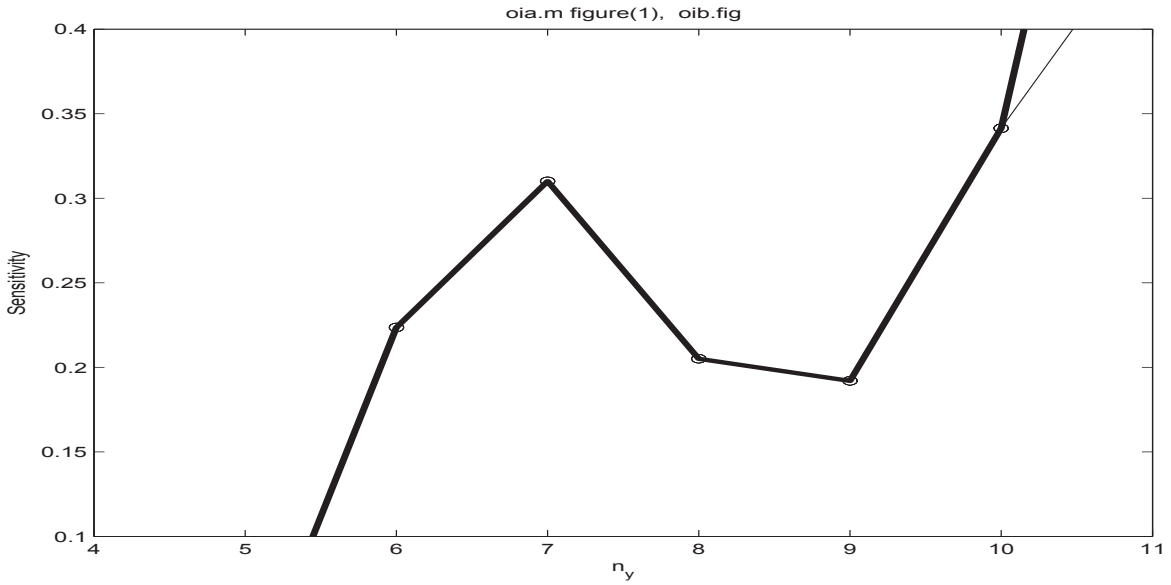

Figure 8: The largest eigenvalues in modulus for a fixed uncertainty in dependence on n_y

3.3 MPC Sensitivity versus Prediction Horizon

Searching for an upper limit of the sensitivity would be desirable in order to get a simpler design facility. However, the large-scale behavior of the result Eq.(19) heavily depends on the power m; for small or big T_a. High T_a causes a decrease versus m in Fig. 9, low T_a an increase in Fig. 10.

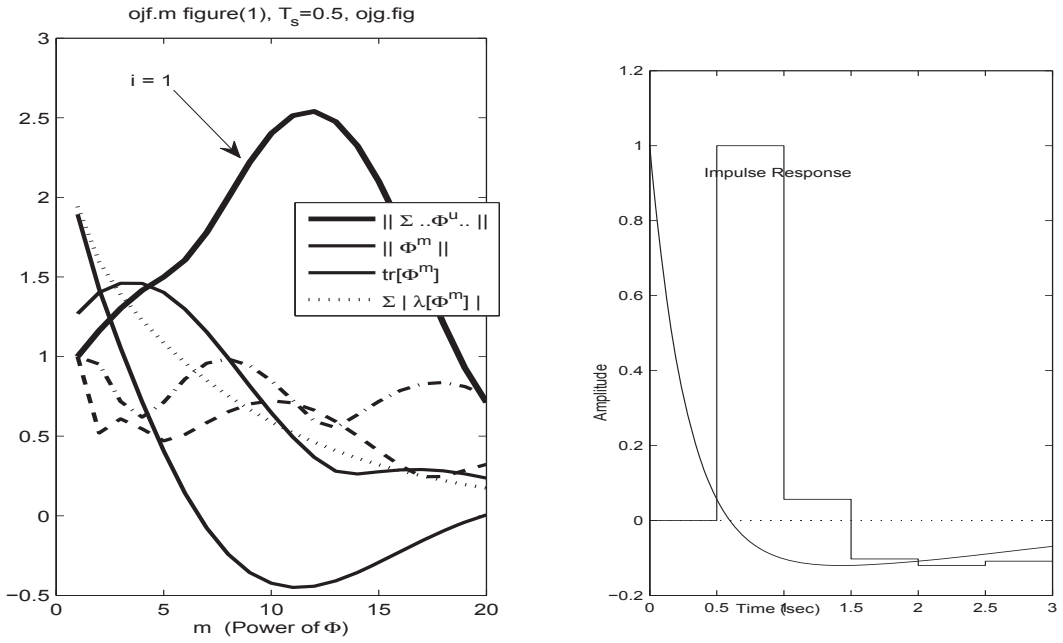

Figure 9: System properties for $T_s = 0.5$. Discrete-time response one sample delayed. (dashdot $i = 2$; dashed $i = 3$)

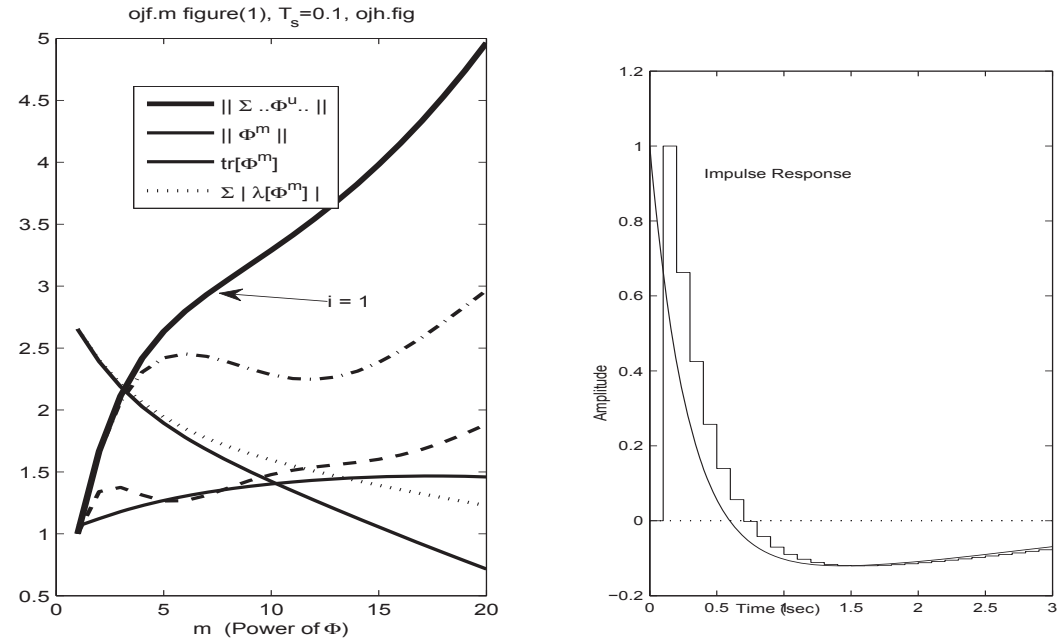

Figure 10: System properties for $T_s = 0.1$ Discrete-time response one sample delayed. (dashdot $i = 2$; dashed $i = 3$)

3.4 Matrix Power Sensitivity

The result of Eq.(17) in powers of $\mathbf{\Phi} = \mathbf{exp}(\mathbf{A} \cdot \mathbf{T_s})$ is depicted versus the power m. An example of $\mathbf{A}$ in phase varable form is selected with $\mathbf{p} = (-1, \quad -2, \quad -3)$ in the last row. The resulting maximum values tend to higher m and T_s , as shown in Figs. 11, 12 and 13.

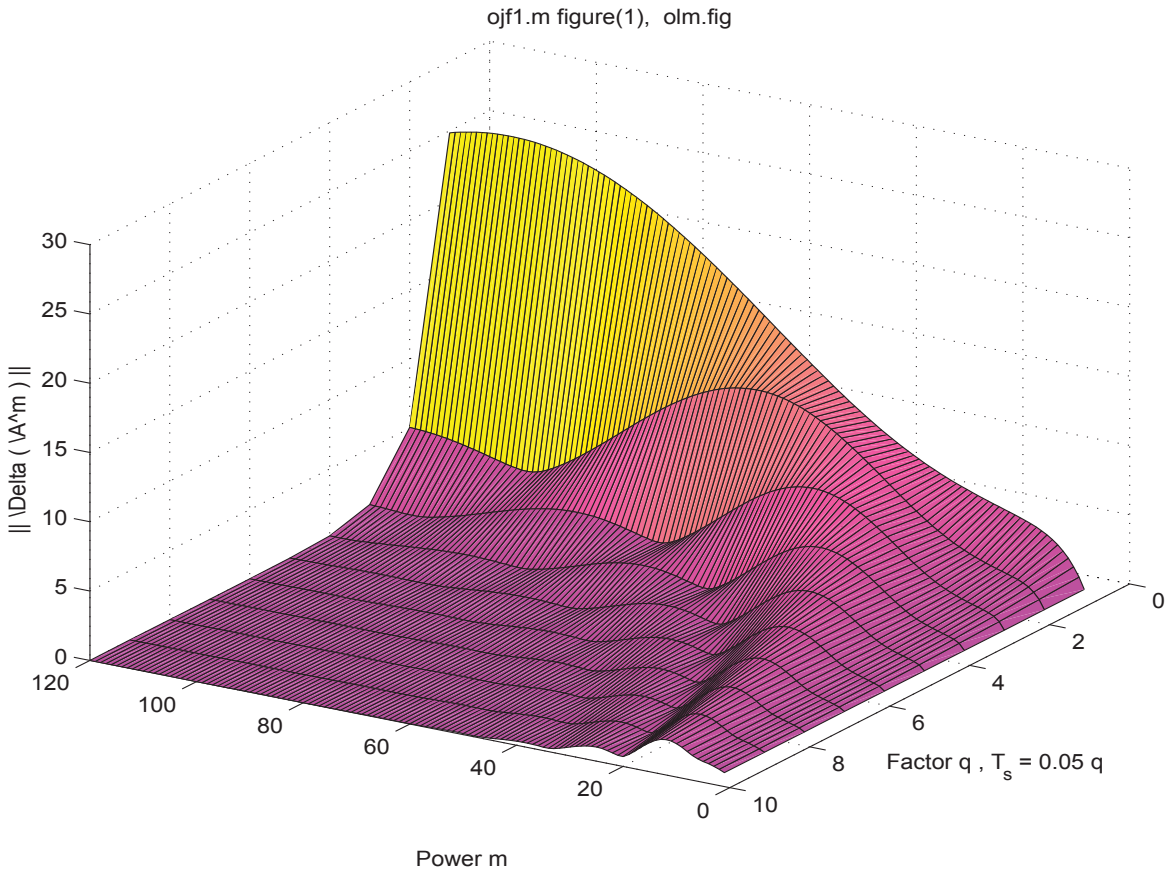

Figure 11: Sensitivity with respect to p_1

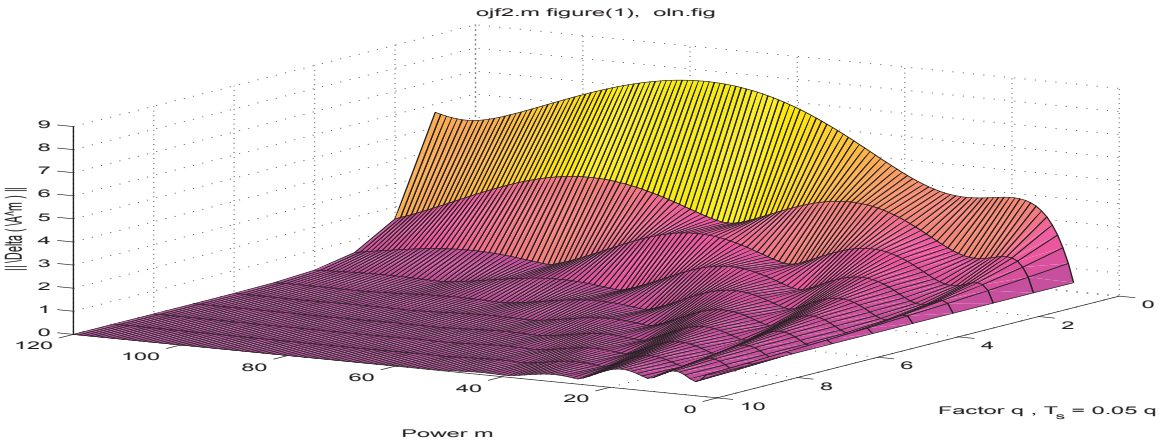

Figure 12: Sensitivity with respect to p_2

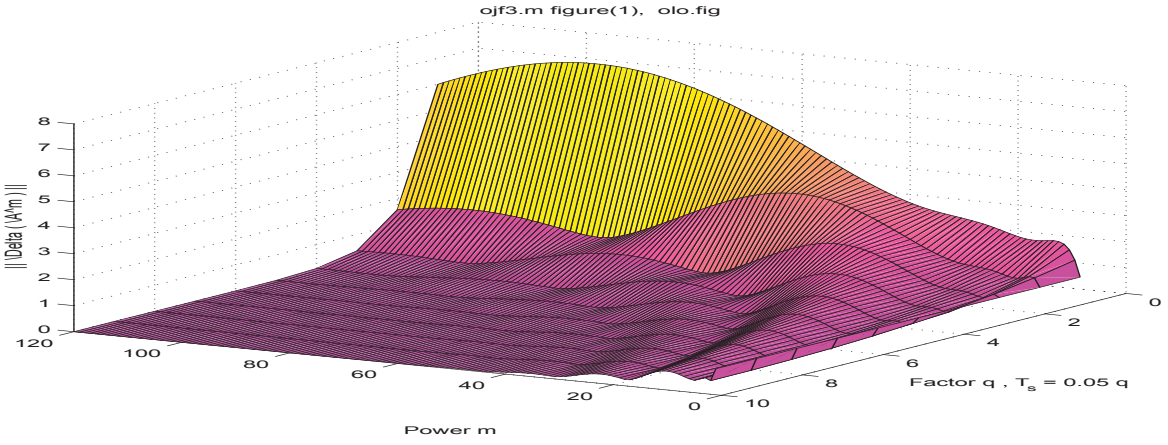

Figure 13: Sensitivity with respect to p_3

4 Balancing Uncertainty versus Prediction Horizon

For the example Eq.(1) two parameters $\Phi(2,1)$ and $\Phi(4,1)$ are considered perturbed. The influence on the spectral norm of $\mathbf{K}_P$ and the norm of its gradients is presented in Figs. 14 to 16. The minimum basis line of the graph turns roughly 90 degrees if the prediction horizon is changed from 6 to 9. The location of the uncertainties has strong influence and is, thus, compensated by the appropriate selection of the horizon; presupposing that it is compatible with the all the given control requirements.

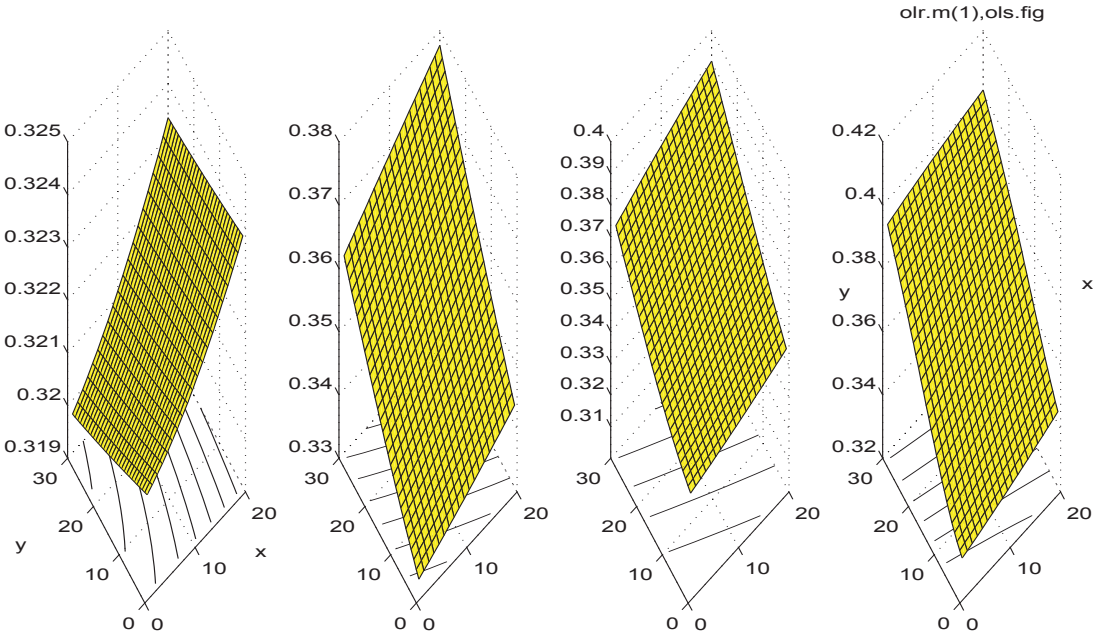

Figure 14: Norm of $\mathbf{K}_P$ versus uncertainty parameters $\Phi(2,1)$ and $\Phi(4,1)$ with 30 and 20 steps, respectively, steps of size 0.01, i.e.,

$x = \Phi(2,1) = 0.4 + 0.01 * xx;\ xx = [1:30]; \qquad y = \Phi(4,1) = 0.4 + 0.01 * yy;\ yy = [1:20]$

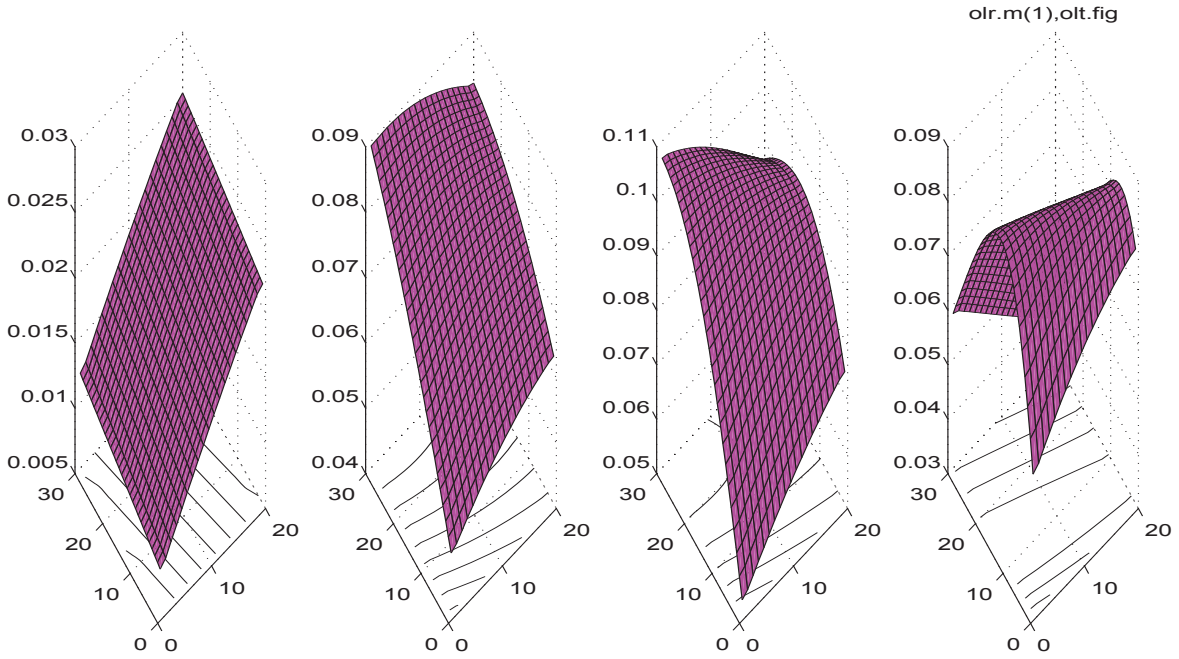

Figure 15: Norm of the gradient $\partial \mathbf{K}_P / \partial \Phi(2,1)$ versus uncertainty parameters $\Phi(2,1)$ and $\Phi(4,1)$ with 30 and 20 steps of 0.01, respectively

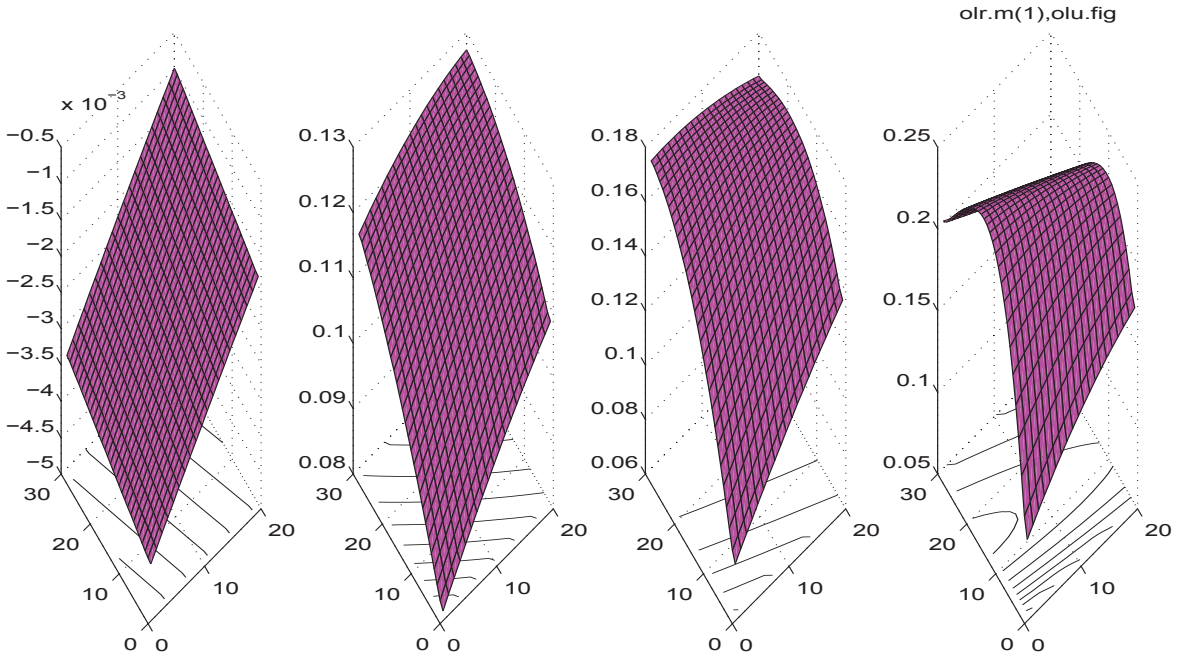

Figure 16: Norm of the gradient $\partial \mathbf{K}_P / \partial \Phi(4,1)$ versus uncertainty parameters $\Phi(2,1)$ and $\Phi(4,1)$ with 30 and 20 steps of 0.01, respectively

5 Spherical Uncertainties and Prediction Horizon

Consider the sixth-order system of the preceding section and a two-valued spherical uncertainty $\mathbf{a}$ of additive type, corresponding to the perturbations of $\Phi(2,1)$ and $\Phi(4,1)$. The norm of the uncertainties is a_0. Then, with the gradient $\partial I_n/\partial \mathbf{a}$ in Eq.(24) the factor $\alpha = a_0/\|\partial I_n/\partial \mathbf{a}\|_F$ yields the local uncertainty $\alpha \cdot \partial I_n/\partial \mathbf{a}$. In this special example, the results are remarkably dependent on n_y. This effect provides an explicit method to adapt n_y in order to select low uncertainty influence. The Fig. 17 depicts the dependence on n_y, located at a cylindric hull. Another remarkalbe result can be observed: the effect above holds for a wide range $-0.2 \leq \Phi(1,6) \leq 0.2$. The results at the borders ± 0.2 are given in Fig. 18.

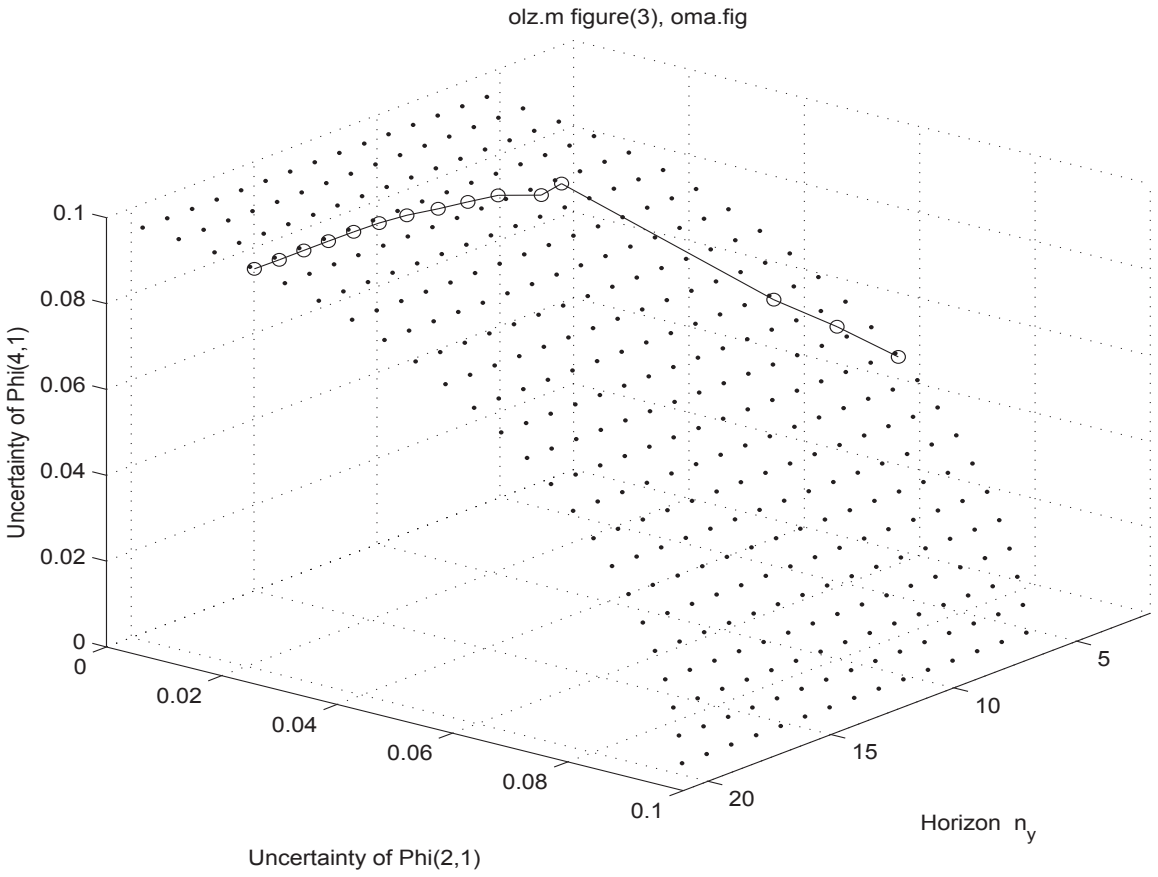

Figure 17: Change of dominant uncertainties (on a cylindric hull) when the prediction horizon n_y is varied

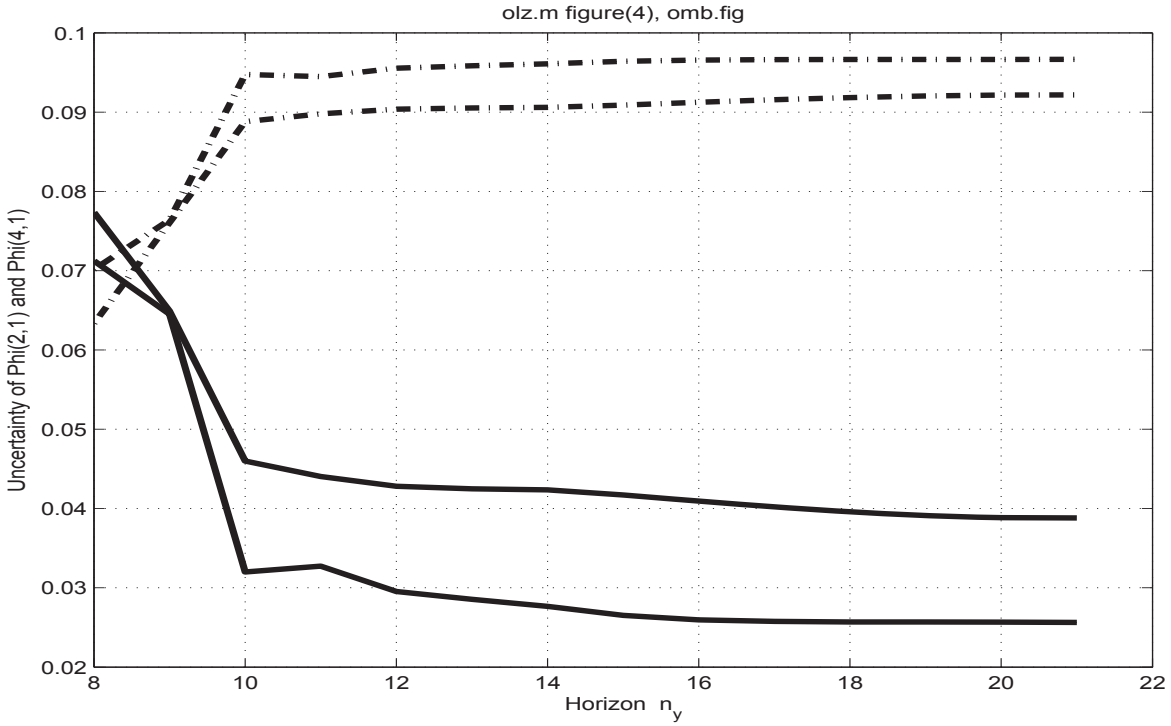

Figure 18: Uncertainties versus n_y at the borders

Conclusion

Several opportunities are reported to include, with low effort, robustness considerations in Model Predictive Control applications. Usually, optimum robustness benefit can be expected in a medium region of the prediction horizon.

References

Adamy, J., 2009, Nichtlineare Regelungen, Berlin: Springer

Bordeneuve-Guibé, J., and Vaucoret, C., 2001, Robust multivariable predictive control, *IEEE Control Systems Magazine* **21**, No.2, pp. 54-65

Camacho, E.F., and Bordons, C., 1999 and 2007, Model predictive control, London: Springer

Demircioglu, H., and Karasu, E., 2000, Generalized predictive control, *IEEE Control Systems Magazine* **20**, No. 5, pp. 36-47

Mattingley, J., Wang, Y., Boyd, S., 2011, Receding horizon control, automatic generation of high-speed solvers, *IEEE Control Systems Magazine* **31**, No. 3, pp. 52-65

Rawlings, J.B., 2000, Tutorial overview of model predictive control, *IEEE Control Systems Magazine* **20**, No. 3, pp. 38-52

Wang, L., 2009, Model predictive control system design and implementation in MATLAB, London: Springer

Weinmann, A., 2012, Performance gradients in automatic control analysis. A catalogue of correspondences. Second edition. *Int. J. Automation Austria* **20**, pp. 1-100. See http://www.acin.tuwien.ac.at/de/Publikationen/Zeitschriften/IJAA

Appendix

A Differential Quotient with Respect to a Matrix Increment

$$\sum_{i=0}^{n} \mathbf{\Phi}^i \equiv (\mathbf{I} - \mathbf{\Phi}^{n+1})(\mathbf{I} - \Phi)^{-1} \tag{12}$$

$$\frac{\partial \mathbf{A}^m}{\partial a_{ij}} = \sum_{k=0}^{k=m-1} \mathbf{A}^k \mathbf{E}_{ij} \mathbf{A}^{m-k-1}, \qquad \mathrm{tr}[\frac{\partial \mathbf{A}^m}{\partial a_{ij}}] = m \ \mathrm{tr}[\mathbf{A}^{m-1}\mathbf{E}_{ij}] \ . \tag{13}$$

For n an integer positive or negative, note

$$\lambda[\mathbf{Z}^n] \equiv (\lambda[\mathbf{Z}])^n \ , \quad \det[\mathbf{Z}^n] \equiv (\det[\mathbf{Z}])^n \ , \quad \mathrm{tr}[\mathbf{Z}^n] \neq (\mathrm{tr}[\mathbf{Z}])^n \ . \tag{14}$$

For $\Delta\mathbf{A} \ll \mathbf{A} \in \mathcal{R}^{n\times n}$

$$(\mathbf{A} + \Delta\mathbf{A})^m \doteq |_{m=3} \mathbf{A}^3 + \mathbf{A}^2 \cdot \Delta\mathbf{A} + \mathbf{A} \cdot \Delta\mathbf{A} \cdot \mathbf{A} + \Delta\mathbf{A} \cdot \mathbf{A}^2 \ . \tag{15}$$

For arbitrary m,

$$(\mathbf{A} + \Delta\mathbf{A})^m \doteq \mathbf{A}^m + \sum_{i=1}^{m} \mathbf{A}^{m-i} \cdot \Delta\mathbf{A} \cdot \mathbf{A}^{i-1} \tag{16}$$

$$\Delta(\mathbf{A}^m) \doteq \sum_{i=1}^{m} \mathbf{A}^{m-i} \cdot \Delta\mathbf{A} \cdot \mathbf{A}^{i-1} \ . \tag{17}$$

$$\begin{aligned} \frac{\partial(\mathbf{A} + \Delta\mathbf{A})^m}{\partial \Delta\mathbf{A}} &\overset{(20)}{\doteq} |_{m=3}(\mathbf{I}_n \otimes \mathbf{A}^2)\frac{\partial \Delta\mathbf{A}}{\partial \Delta\mathbf{A}} + (\mathbf{I}_n \otimes \mathbf{A})\frac{\partial(\Delta\mathbf{A} \cdot \mathbf{A})}{\partial \Delta\mathbf{A}} + \frac{\partial \Delta\mathbf{A}}{\partial \Delta\mathbf{A}}(\mathbf{I}_n \otimes \mathbf{A}^2) \qquad (18) \\ &\doteq |_{m=3}(\mathbf{I}_n \otimes \mathbf{A}^2)\frac{\partial \Delta\mathbf{A}}{\partial \Delta\mathbf{A}} + (\mathbf{I}_n \otimes \mathbf{A})\frac{\partial \Delta\mathbf{A}}{\partial \Delta\mathbf{A}}(\mathbf{I}_n \otimes \mathbf{A}) + \frac{\partial \Delta\mathbf{A}}{\partial \Delta\mathbf{A}}(\mathbf{I}_n \otimes \mathbf{A}^2) \\ &\overset{(21)}{\doteq} \sum_{i=1}^{m}(\mathbf{I}_n \otimes \mathbf{A}^{m-i}) \ \ \bar{\mathbf{U}}^{m^2\times m^2} \ \ (\mathbf{I}_n \otimes \mathbf{A}^{i-1}) \ . \qquad (19) \end{aligned}$$

$$\frac{\partial}{\partial \mathbf{M}}\mathbf{A}(\mathbf{M})\mathbf{B}(\mathbf{M}) = \frac{\partial \mathbf{A}}{\partial \mathbf{M}}(\mathbf{I}_s \otimes \mathbf{B}) + (\mathbf{I}_r \otimes \mathbf{A})\frac{\partial \mathbf{B}}{\partial \mathbf{M}} \qquad \frac{\partial(\mathbf{AB})}{\partial \mathbf{M}} \in \mathcal{R}^{nr \times qs} \ . \tag{20}$$

$$\frac{\partial \mathbf{M}^{(k\times l)}}{\partial \mathbf{M}} = \bar{\mathbf{U}}_{k,l} = \bar{\mathbf{U}}_{k,l}^{(k^2 \times l^2)} \triangleq \sum_{i=1}^{k}\sum_{j=1}^{l} \mathbf{E}_{ij}^{(k\times l)} \otimes \mathbf{E}_{ij}^{(k\times l)} \ . \tag{21}$$

B Basics of Model Predictive Control

The actuating variable is separated into the previous one and an increment $\mathbf{u}(k) = \mathbf{u}(k-1)+\Delta\mathbf{u}(k)$. The predicted values are concatenated in partitioned vectors. Thus, $\hat{\mathbf{y}}(k+1|k)$ (or abbreviated $\hat{\mathbf{y}}(k+1)$) is a vector including all the predicted $\mathbf{y}(k+i)$ based on the information at sampling time kT_s. That is,

$$\hat{\mathbf{y}}(k+1) \triangleq \begin{pmatrix} \mathbf{y}(k+1) \\ \mathbf{y}(k+2) \\ \vdots \\ \mathbf{y}(k+n_y) \end{pmatrix}, \quad \hat{\mathbf{y}}_{ref}(k+1) \triangleq \begin{pmatrix} \mathbf{y}_{ref}(k+1) \\ \mathbf{y}_{ref}(k+2) \\ \vdots \\ \mathbf{y}_{ref}(k+n_y) \end{pmatrix}, \quad \Delta\hat{\mathbf{u}}(k+1) \triangleq \begin{pmatrix} \Delta\mathbf{u}(k+1) \\ \Delta\mathbf{u}(k+2) \\ \vdots \\ \Delta\mathbf{u}(k+n_u-1) \end{pmatrix}, \tag{22}$$

where $\hat{\mathbf{y}}_{ref}$ is the predicted horizon n_y of the reference values, and n_u is the horizon of the actuating variable increments $\Delta\mathbf{u}(k)$ (*Camacho, E.F., and Bordons, C., 2007; Demircioglu, H., and Karasu, E., 2000; Adamy, J., 2009; Wang, L., 2009*). The method is also known as Receding Horizon Control (*Mattingley, J., et al., 2011*). The dimensions are

$$\hat{\mathbf{y}}(k+1), \quad \hat{\mathbf{y}}_{ref}(k+1), \quad \hat{\mathbf{r}}_d(k) \in \mathcal{R}^{rn_y}, \quad \Delta\hat{\mathbf{u}}(k) \in \mathcal{R}^{mn_u} \ . \tag{23}$$

Using a square index of performance

$$I_n(\Delta\hat{\mathbf{u}}(k)) = \hat{\mathbf{y}}(k+1)^T\mathbf{Q}\hat{\mathbf{y}}(k+1) + \Delta\hat{\mathbf{u}}^T\mathbf{R}\Delta\hat{\mathbf{u}} \tag{24}$$

for the error signal horizon (reference minus output based on $\mathbf{x}(k)$ and $\mathbf{u}(k-1)$) and the actuating variable increments $\Delta\hat{\mathbf{u}}(k)$, the weighting matrices $\mathbf{R} \in \mathcal{R}^{mn_u \times mn_u}$ and $\mathbf{Q} \in \mathcal{R}^{rn_y \times rn_y}$, respectively, and its partial derivative with respect to $\Delta\hat{\mathbf{u}}(k)$,

$$\frac{\partial I_n}{\partial \Delta\hat{\mathbf{u}}} = \mathbf{0} \quad \rightsquigarrow \text{Eq.(27)}, \tag{25}$$

one finds the optimum result

$$\hat{\mathbf{r}}_d(k) = \mathbf{F}_P\ \mathbf{x}(k) + \mathbf{G}_P\ \mathbf{u}(k-1) - \hat{\mathbf{y}}_{ref}(k+1) \tag{26}$$

$$\Delta\hat{\mathbf{u}}(k) = -(\mathbf{H}_P^T\mathbf{Q}\mathbf{H}_P + \mathbf{R})^{-1}\mathbf{H}_P^T\mathbf{Q}\ \hat{\mathbf{r}}_d(k) \tag{27}$$

$$\mathbf{u}(k) = \mathbf{u}(k-1) + \mathbf{K}_P\ [\hat{\mathbf{y}}_{ref}(k+1) - \mathbf{F}_P\ \mathbf{x}(k) - \mathbf{G}_P\ \mathbf{u}(k-1)] \tag{28}$$

$$\hat{\mathbf{y}}(k+1) = \mathbf{F}_P\ \mathbf{x}(k) + \mathbf{G}_P\ \mathbf{u}(k-1) - \mathbf{H}_P(\mathbf{H}_P^T\mathbf{Q}\mathbf{H}_P + \mathbf{R})^{-1}\mathbf{H}_P^T\mathbf{Q}\ \hat{\mathbf{r}}_d(k) \ . \tag{29}$$

Starting with some initials $\mathbf{x}(k),\ \mathbf{u}(k-1),\ \hat{\mathbf{y}}_{ref}(k+1)$ the equations are used in the following order to find $I_n(\Delta\hat{\mathbf{u}}(k))$: Eq.(26), Eq.(27), Eq.(29), Eq.(24).

For the receding horizon assumption, the solution steps are similar to those for linear-quadratic controllers and Riccati-equation-like results.

The partitioned matrices in use are

$$\mathbf{F}_P \stackrel{\triangle}{=} \begin{pmatrix} \mathbf{C\Phi} \\ \mathbf{C\Phi}^2 \\ \vdots \\ \mathbf{C\Phi}^{n_y} \end{pmatrix} \in \mathcal{R}^{rn_y \times n}, \qquad \mathbf{G}_P \stackrel{\triangle}{=} \begin{pmatrix} \mathbf{C\Psi} \\ \mathbf{C}(\mathbf{\Phi}+\mathbf{I})\mathbf{\Psi} \\ \vdots \\ \mathbf{C}(\mathbf{\Phi}^{n_y-1}+\ldots+\mathbf{I})\mathbf{\Psi} \end{pmatrix} \in \mathcal{R}^{rn_y \times m}, \quad (30)$$

$$\mathbf{G}_P \stackrel{(12)}{=} \mathbf{C} \begin{pmatrix} \mathbf{I}-\mathbf{\Phi} \\ \mathbf{I}-\mathbf{\Phi}^2 \\ \mathbf{I}-\mathbf{\Phi}^3 \\ \vdots \\ \mathbf{I}-\mathbf{\Phi}^{n_y} \end{pmatrix} (\mathbf{I}-\mathbf{\Phi})^{-1}\mathbf{\Psi} \ . \quad (31)$$

$$\mathbf{H}_P \stackrel{\triangle}{=} \begin{pmatrix} \mathbf{C\Psi} & \mathbf{0} & \ldots & \mathbf{0} \\ \mathbf{C}(\mathbf{\Phi}+\mathbf{I})\mathbf{\Psi} & \mathbf{C\Psi} & \ldots & \mathbf{0} \\ \mathbf{C}(\mathbf{\Phi}^2+\mathbf{\Phi}+\mathbf{I})\mathbf{\Psi} & \mathbf{C}(\mathbf{\Phi}+\mathbf{I})\mathbf{\Psi} & \ldots & \mathbf{0} \\ \vdots & \vdots & \ddots & \vdots \\ \mathbf{C}(\mathbf{\Phi}^{n_y-1}+\ldots+\mathbf{I})\mathbf{\Psi} & \mathbf{C}(\mathbf{\Phi}^{n_y-2}+\ldots+\mathbf{I})\mathbf{\Psi} & \ldots & \mathbf{C}(\mathbf{\Phi}^{n_y-n_u}+\ldots+\mathbf{I})\mathbf{\Psi} \end{pmatrix} \in \mathcal{R}^{rn_y \times mn_u}, \quad (32)$$

$$\mathbf{K}_P = (\mathbf{I}_m \vdots \mathbf{0}^{[m\times(m-1)n_u]}) \ \left[\ (\mathbf{H}_P^T\mathbf{Q}\mathbf{H}_P+\mathbf{R})^{-1}\mathbf{H}_P^T\mathbf{Q}\ \right] \quad \in \mathcal{R}^{m\times rn_y} \ . \quad (33)$$

The matrix $\mathbf{H}_P$ results from the shifted matrices $\mathbf{G}_P$ which is performed via operator `locfunc`.

Dr. Norbert Rozsenich
Österreichische Gesellschaft für
Automatisierungs- und Robotertechnik

Reisebericht IFAC-IAV 2013, Brisbane

Veranstalter: International Federation of Automatic Control (IFAC)

Konferenztitel: Intelligent Autonomous Vehicles Symposium 2013 (IAV 2013)

Zeit: 26. – 28. Juni 2013, Brisbane/Gold Coast, Australien

Teilnehmerzahl: ca. 110 (davon 2 aus Österreich)

Vorsitzender des Programmkomitees: Univ.-Prof. Dr. Stefan Jakubek, Institut für Mechanik und Mechatronik, TU Wien

Organisator: Univ.-Prof. Dr. Ljubo Vlacic, Institute for Intelligent and Integrated Systems, Griffith University Lecce, Brisbane/Gold Coast

==========

Als intelligentes autonomes Fahrzeug (englische Abkürzung: IAV) bezeichnet man ein Fahrzeug, das frei (also ohne menschliche Unterstützung) navigiert. Derartige Fahrzeuge können mit Hilfe verschiedener Sensoren ihre Umgebung wahrnehmen und aus den gewonnenen Informationen ihre Position bestimmen, ein Ziel ansteuern und Kollisionen auf dem Weg vermeiden. Autonome Fahrzeuge sind nicht gleichzusetzen mit unbemannten Fahrzeugen, da letztere in der Regel nicht frei navigieren sondern von Menschen ferngesteuert werden.

Die IAV 2013 bot ein exzellentes Forum zur Präsentation und zur Diskussion neuester F&E-Ergebnisse aus dem Bereich „Intelligente autonome Fahrzeuge und Systeme“. Die Vortragenden waren Forscher, Entwickler und Ingenieure aus den Sektoren

- Intelligente autonome Landfahrzeuge
- Intelligente autonome Flugzeuge und Flugkörper
- Intelligente autonome maritime Fahrzeuge
- Grundlagen der IAV-spezifischen Steuerungs- und Regelungstechnik unter besonderer Berücksichtigung der Sensorik und Aktuatorik

Die vier Plenarvortragenden behandelten folgende vier Themen:

- Autonome Flugkörper mit Überschallgeschwindigkeit um die 5.000 km/h (Allan Paull, Defense Science & Technology Organistion, Australia)
- Zeitkritische kooperative Streckenoptimierung von Fahrzeugkolonnen (Isaac Kaminer, Department of Mechanical and Aerospace Engineering, Naval Post-Graduate School, Monterey, Canada)
- Trends und Technologien für autonome kooperative Automobile (Christoph Stiller, Institut für Mess- und Regelungstechnik, Karlruhe)
- Robuste Autonomiestrategien für intelligente Land- und Luftfahrzeuge (Tristan Perez, School of Engineering, University of Newcastle, New South Wales, Australia)

Verfestigt wurde mein Eindruck, dass wesentliche technologische Errungenschaften (vor allem in der Sensor- und Steuerungstechnik) für die zivile Forschung und Entwicklung im IAV-Bereich auf Erfahrungen und Ergebnissen der militärischen Forschung aufbauen. Auf der IAV 2013 war durch die Themen zahlreicher einschlägiger Vorträge eine starke Achse zwischen USA, Australien und Kanada bei militärischen IAV-Projekten erkennbar.

Für die österreichische Forschungs- und Technologieszene besonders interessant waren die Ausführungen von Christoph Stiller (Karlsruhe). Er gab in seinem Plenarvortrag einen guten Überblick über den Stand der Entwicklung und der Realisierung von autonomen Landfahrzeugen und skizzierte viele aktuelle und teilweise noch offene Forschungsthemen, z.B. die unter den Bedingungen höchster Zuverlässigkeit noch immer nicht optimal gelösten Fragen der Interaktion der sensorgestützten Erkennung der Fahrzeugumgebung und den im Fahrzeug und seine Prozessoren integrierten Entscheidungsalgorithmen.

Für aktuelle österreichische Forschungsarbeiten im Themenbereich „Urbane Elektromobilität“ waren vor allem einige Vorträge aus folgenden zwei Untergruppen von Interesse:

- WeB1 (Autonomous Road Vehicles & Traffic Control)
- ThB1 (Autonomous Land Vehicles)

Besonders spannend fand ich den Vortrag von Kim Junsoo (Hanyang University, Seoul) über Algorithmen zur Streckenplanung von Landfahrzeugen in komplexen Umgebungen. Kim Junsoo arbeitet mit seinem Team an der Hanyang Universität intensiv mit der Hyundai Motor Group in Südkorea zusammen und konnte bereits etliche internationale Preise gewinnen.

Obwohl viele mathematische Grundlagen und raffinierte Computeralgorithmen ursprünglich von europäischen oder südostasiatischen Wissenschaftern entwickelt wurden, scheinen die USA aber technologisch im Themenbereich „Autonome Landfahrzeuge“ einen spürbaren Vorsprung zu besitzen. Ein Indiz dafür ist die Tatsache, dass dem Internetunternehmen Google nach mehreren Jahren der Entwicklung bereits im Dezember 2011 ein US-Patent für die Technik zum Betrieb von autonomen Fahrzeugen gewährt wurde. Die Google-Testflotte hatte nach Aussage des Unternehmens zu diesem Zeitpunkt bereits ca. 257.000 km (160.000 Meilen) unter begrenzter Einwirkung des Fahrers sowie mehr als 1.600 km (1.000 Meilen) ohne Fahrerbeteiligung zurückgelegt. Einige Konferenzteilnehmer bewerteten das Vorgehen von Google als großen Schritt zu einem baldigen kommerziellen Einsatz der Technik in Fahrzeugen. Im Mai 2012 erhielt Google die erste Zulassung eines autonomen Fahrzeugs in den USA. So erlaubte der US-Bundesstaat Nevada den Test des selbstfahrenden Autos auf öffentlichen Straßen. Bedingung ist jedoch, dass sich eine Person hinter dem Steuer befindet, die notfalls eingreifen kann. Google hat sich im August 2013 angeblich am Taxidienst Uber beteiligt und soll - in Kooperation mit Autoherstellern – beabsichtigen, ein Robotaxi zu bauen, das Fahrgäste selbsttätig transportiert.

Während der Konferenz habe ich auch versucht, mit einigen Teilnehmern aus Europa ins Gespräch zu kommen, um mein Bild von den einschlägigen F&E-Arbeiten in Europa auf den neuesten Stand zu bringen. Hier einige Eindrücke:

Es gibt offensichtlich in Europa zahlreiche Forschungsarbeiten zu autonomen Fahrzeugen, so z. B. das Projekt „Stadtpilot“ an der TU Braunschweig oder das Projekt „Spirit of Berlin“ am Forschungsbereich „Künstliche Intelligenz“ der Freien Universität Berlin. Im September 2011 wurde das Autonome Fahrzeug "Made in Germany" der FU Berlin getestet. Es fuhr mehrere Kilometer im Verkehr von Berlin. Es steuerte über Kreisverkehre und Ampeln. In Zusammenarbeit mit dem TÜV Nord wurde die Strecke erarbeitet und ein Sicherheitskonzept erstellt.

Im Rahmen des Projekts Cybercars-2 hat das Institut für Parallele und Verteilte Systeme der Universität Stuttgart gemeinsam mit Forschungseinrichtungen und anderen Partnern aus dem In- und Ausland derartige autonome Fahrzeuge entwickelt und testet sie. Die Stuttgarter Wissenschaftler untersuchen, wie ganze Scharen von solchen Fahrzeugen zusammenarbeiten könnten, um einen sicheren und komfortablen Personentransport zu gewährleisten. Ein wichtiger Aspekt dabei ist die Kooperation zwischen den Fahrzeugen. Diese sollen nicht starr an vorgefertigten Fahrplänen festhalten, sondern ihre Wege selbst planen dürfen. Dabei spielt die Absprache untereinander eine große Rolle. Jedes Fahrzeug kann jederzeit mit jedem anderen Kontakt aufnehmen, Verkehrsinformationen austauschen oder Bitten und Anfragen stellen. Welches Fahrzeug zum Beispiel

an einer Kreuzung zuerst fahren darf, wird nicht mehr von starren Regeln bestimmt, sondern wird während der Fahrt zwischen den Fahrzeugen verhandelt. So erhält beispielsweise ein Fahrzeug freie Fahrt über alle Kreuzungen, um damit eine Verspätung auszugleichen. Die Forscher entwickeln im Projekt Cybercars-2 nicht nur Kommunikationssysteme, sondern auch Verhandlungs- und Entscheidungsprotokolle. Denn gerade bei vielen Fahrzeugen in großen Verkehrsnetzen können schnell Konflikte, Staus und Blockaden entstehen. Im Rahmen des Projekts Cybercars-2 bauten die Wissenschaftler zehn echte autonome Fahrzeuge in fünf unterschiedlichen Typen und setzten sie erfolgreich innerhalb eines Demonstrationssystems ein. Für die Zukunft sind auch sehr viel größere Systeme denkbar. Allerdings ist nicht jede Fahrstrategie, die mit zehn Fahrzeugen funktioniert, auch für hundert oder tausend Autos geeignet. Die Gruppe Bildverstehen am Institut für Parallele und Verteilte Systeme der Universität Stuttgart hat deshalb einen speziellen Simulator für die Cybercars-Fahrzeuge entwickelt, in dem beliebig große Verkehrssysteme mit beliebig vielen Fahrzeugen simuliert werden können. Damit ist es möglich, auch komplexe Verkehrssituationen mit zahlreichen miteinander kommunizierenden Fahrzeugen zu untersuchen. Nur wenn eine Fahrstrategie sich auch unter diesen schwierigen Bedingungen bewährt, ist sie auch für den sicheren Betrieb der realen Fahrzeuge geeignet.

Um die Entwicklung derartiger Fahrzeuge voranzutreiben, gab es früher einige Leistungsvergleiche, so z. B. den European Land Robot Trial und der DARPA Grand Challenge. Der DARPA Grand Challenge wurde aber 2007 aus mir nicht bekannten Gründen eingestellt.

Auf der Internationalen Automobilausstellung (IAA) in Frankfurt zeigten 2013 Autobauer aus der ganzen Welt, was sie können und welche Visionen sie für die mobile Zukunft haben. So stellte z.B. Mercedes-Benz ein als „Intelligent Drive“ bezeichnetes System vor, mit dem die Autos bald vollständig autonom über die Straßen fahren sollen. Auf der Teststrecke zwischen Mannheim und Pforzheim wurden teilautonome Mercedesautos der S-Klasse getestet, bei denen ein proprietäres Navigationsgerät zum Einsatz kam, das eine um ein Vielfaches höhere Genauigkeit als ein herkömmliches System aufweist und das allerdings genau für diese Strecke optimiert wurde. Es handelt sich dennoch um eine beeindruckende Ingenieursleistung

Nach dem derzeitigen „E-Mobility-Hype“ in Europa und speziell in Österreich werden meiner Einschätzung nach autonome Fahrzeuge der nächste technologische Meilenstein sein und unsere Art der Mobilität radikal verändern. Die Hoffnungen sind groß. Könnten doch die Unfallzahlen auf einen noch nie dagewesenen Tiefpunkt rutschen, wenn autonome Fahrzeuge die Regel sind. Bis dahin ist es allerdings noch ein weiter Weg. Das Institute of Electrical and Electronics Engineers (IEEE) prognostiziert, dass im Jahr 2040 bis zu 75

Prozent aller Fahrzeuge vollkommen autonom unterwegs sein werden. Z.B. sieht die Roadmap der in Hannover beheimateten Continental AG vor, dass ab dem Jahr 2016 teilautomatisierte Systeme in Serie produziert werden können, die insbesondere im Stadtverkehr bis zu 30 km/h das nervige Anfahren und Anhalten im Stau dem ins Fahrzeug eingebauten Automaten übergeben.

Nach Einschätzung vieler Vortragender, mit denen ich bei der IAV 2013 in Brisbane diskutieren konnte, ist damit zu rechnen, dass ab dem Jahr 2020 automatisierte Fahrzeuge verfügbar sein werden, die autonom auch über 30 km/h fahren können, allerdings noch nicht auf der Autobahn einsetzbar sind. Für hohe Geschwindigkeiten soll zu dieser Zeit noch immer der Fahrzeugführer das Steuer in der Hand halten. Erst ab 2025 soll es soweit sein, und die ersten vollautomatisierten Fahrzeuge könnten dann auch bei Geschwindigkeiten von über 130 km/h das Steuer übernehmen. Während der Konferenz wurde aber übereinstimmend betont, dass man auf dem Weg zur Vollautomatisierung den Fahrer niemals entmündigen werde. Jeder Zeit muss der Fahrer (nach dem Muster des Autopilotsystems in Flugzeugen) die volle Kontrolle über Gaspedal, Bremse und Lenkrad übernehmen können. In diesem Zusammenhang wurde auch über die bisher kaum beachtete Problematik diskutiert, dass es Hackerangriffe auf solche Fahrzeuge geben könnte. Eine Horrorvorstellung, dass ein Hacker eines oder mehrere Fahrzeuge übernehmen und vom heimischen Rechner aus lenken könnte. Oder gar, dass mit feindlich übernommenen Fahrzeugen Anschläge (fremd gesteuertes Fahrzeug beschleunigt und rast mit Vollgeschwindigkeit in eine Fußgängerzone oder Menschenmenge) begangen werden. Die Hersteller von künftigen autonomen Fahrzeugen müssen daher vorsorgen, dass die Verbindung über das Internet komplett vom restlichen Motormanagement getrennt ist und bleibt – nicht nur durch digitale Schranken, sondern tatsächlich mit physischen Grenzen.

International Stability, Technology and Culture

(SWIIS 2013)

IFAC Workshop

Prishtina (Republic of Kosovo)

June 6-8, 2013

The University for Business and Technology (UBT) organized this IFAC Workshop in cooperation with the Department of Intelligent Handling and Robotics (IHRT) of Vienna University of Technology which took place from June 6 to 8, 2013 at UBT in Prishtina (Kosovo).

Main sponsor was the IFAC TC 9.5 (TECIS), Co-sponsors the IFAC TC's 9.1, 9.2, 9.3 and 9.4.

The main goal of this event was to offer members of the scientific community predominantly from Kosovo, Albania and Macedonia the possibility to present their scientific research results in an international recognized event.

The program consists of two survey papers and 47 contributed papers arranged in 10 technical and 2 invited sessions.

One of the survey papers "From Engineering to Mechatronics Management" was a report of the development and realisation of a "Mechatronics Management" BSc and MSc program at the UBT. This program is based on a "Engineering Management" program running at Vienna University of Technology since 1995. First experiences of the currently running program were outlined and shortly discussed.

The other survey paper given by P. Groumpos "An Overview of the Triangle of Knowledge as a Driving Force for Sustainable Growth in Developing Nations" gave an overview about different philosophies of connections between education, research and innovation.

As an historic tradition in SWIIS the subjects of the papers covered the field from globalization impact on international stability via knowledge Society vs. International Stability and Complex Adaptive Systems to End of Life Management.

One of the invited sessions "Automatic Control Education & International Stability: Lessons from International, Cross-disciplinary, Intercultural Pedagogies" was organized by A. Stapleton (Ireland). The contributions gave an overview about multi-cultural education especially on postgraduate level and the vision of a new Europe-wide University. The other invited session "Re-engineering of process control and maintenance systems" organized by M. Hadjiski (Bulgaria) with 4 papers discussed very interesting topics on Automation of production, mostly chemical, plants.

The working group “End of Life Management” in TC 9.5 was responsible for a session with the same name. The subject of the papers were “Recycling of mobile phones in Kosovo” – a classical topic - and relatively new, “Recover Rare and Precious Metals from WEEE” and “Research and education with Scrap”.

In addition to the program technical visits were organized in a furniture factory, a production plant for medications – owned and managed by a graduate of the Engineering Management Program of UBT.

The 68 attendees from 14 countries enjoyed the social events including a welcome reception, a banquet in the historical town of Vushtrri and a farewell at the new campus of UBT.

Reports of this workshop were in the TV, Broadcast, and several times in daily newspapers.

Because from the 49 papers 16 were from the countries mentioned above the main goal were reached according to the policy of TC 9.5

P. Kopacek

IPC Chair

Instruction to authors – presented as a pattern paper (18 pt)

A. Maier, F. Huber (12 pt)
Department ....., Vienna, Austria

Received April 8, 1999

Abstract
This paper shows …… (italics, 12 pt)

1 General (14 pt)

Authors should prepare their manuscript camera ready, format A 4, 12 typeface and must present their manuscript in good quality. At the left/right edge 2.5 cm, at the top/bottom edge 3 cm. Authors are invited to use papers of this journal as a sample. Please do not use an eraser or erasing fluid. Footnotes should be avoided if possible. Authors are expected to submit their paper to one of the publishers (O.Univ.Prof.Dr. Peter Kopacek, Intelligent Handling Devices and Robotics, Vienna University of Technology, Favoritenstrasse 9-11, A-1040 Vienna, Austria, Fax: +43 1 58801-31899 or O.Univ.Prof.Dr. Alexander Weinmann, Institute of Automation and Control, Vienna University of Technology, Gusshausstr. 27-29, A-1040 Vienna, Austria, Fax: +43 1 58801 37699).

Email address for submitting pdf-manuscripts: weinmann@acin.tuwien.ac.at

2 References (14 pt)

Within the paper references should appear in the following form:
(Mayer, H., 1990) or (*Mayer, H., 1990)* (12 pt);
Mayer, H., 1990, discovered that....

3 Figures and Tables (14 pt)

Figures and Tables should be integrated in the paper and have to be referred to as Fig. 4.1 or Tab. 5.2.

4 References

References are to be listed alphabetically according to first author. (11 pt)

5 Word Processing System/Editor

Microsoft Word 2000 or higher; TeX or LaTeX.

Wenn unzustellbar, retour an:

IFAC-Beirat Österreich (E318 / E376)
Favoritenstraße 9-11, A-1040 Wien /
Gußhausstraße 27-29, A-1040 Wien